

Original Article



OPEN ACCESS

Received: Aug 19, 2024
Revised: Dec 1, 2024
Accepted: Dec 2, 2024
Published online: Dec 17, 2024

*Correspondence to

Sang-Il Lee

Division of Rheumatology, Department of Internal Medicine and Institute of Medical Science, Gyeongsang National University School of Medicine and Gyeongsang National University Hospital, 79 Gangnam-ro, Jinju 52727, Korea.
Email: goldgu@gnu.ac.kr

Suhee Kim

Division of Rheumatology, Department of Internal Medicine and Institute of Medical Science, Gyeongsang National University School of Medicine and Gyeongsang National University Hospital, 79 Gangnam-ro, Jinju 52727, Korea.
Email: vetksh@gmail.com

Copyright © 2024. The Korean Association of Immunologists











This is an Open Access article distributed under the terms of the Creative Commons Attribution Non-Commercial License (<https://creativecommons.org/licenses/by-nc/4.0/>) which permits unrestricted non-commercial use, distribution, and reproduction in any medium, provided the original work is properly cited.

ORCID iDs

Hee Jin Park 
<https://orcid.org/0000-0001-9415-9802>
Dakyum Yu 
<https://orcid.org/0009-0005-3128-6632>
Seong-Tshool Hong 
<https://orcid.org/0000-0001-8254-6581>

<https://immunenetw.org>

Bifidobacterium longum RAPO Attenuates Dermal and Pulmonary Fibrosis in a Mouse Model of Systemic Sclerosis through Macrophage Modulation and Growth of Short-Chain Fatty Acid Producers

Hee Jin Park ¹, Dakyum Yu ¹, Seong-Tshool Hong ², Juyeon Lee ³, Sang-Jun Park ³, Myeong Soo Park ³, Hanna Lee ¹, Mingyo Kim ¹, Yun-Hong Cheon ¹, Seung-Geun Lee ⁴, Dong Hyun Sohn ⁵, Jae-Bum Jun ⁶, Suhee Kim ^{1,*}, Sang-Il Lee ^{1,*}

¹Division of Rheumatology, Department of Internal Medicine and Institute of Medical Science, Gyeongsang National University School of Medicine and Gyeongsang National University Hospital, Jinju 52727, Korea

²Department of Biomedical Sciences and Institute for Medical Science, Chonbuk National University Medical School, Jeonju 54907, Korea

³Research Center, BIFIDO Co, Ltd., Hongcheon 25117, Korea

⁴Division of Rheumatology, Department of Internal Medicine and Biomedical Research Institute, Pusan National University Hospital, Pusan National University School of Medicine, Busan 49241, Korea

⁵Department of Microbiology and Immunology, Pusan National University School of Medicine, Yangsan 50612, Korea

⁶Department of Rheumatology, Hanyang University Hospital for Rheumatic Diseases, Seoul 04763, Korea

ABSTRACT

Systemic sclerosis (SSc) is a complex autoimmune disease with an unclear etiology and no effective treatments. Recent research has suggested involvement of the microbiome in SSc pathogenesis. This study aimed to identify specific microbial species associated with SSc and explore their therapeutic potential. Serum Abs against 384 intestinal microbial species revealed a significant depletion in Abs against *Bifidobacterium longum* in patients with SSc compared to healthy controls. In a bleomycin-induced SSc mouse model, oral administration of *B. longum* strain RAPO attenuated skin and lung fibrosis, accompanied by reduced infiltration of inflammatory monocytes/macrophages and downregulation of pro-inflammatory cytokines and chemoattractant *Ccl2* genes in lymph nodes and fibrotic tissues. *B. longum* RAPO treatment restored fecal microbial diversity and augmented short-chain fatty acid (SCFA)-producing bacteria in the gut, leading to increased fecal butyrate levels and upregulated SCFA receptor *Gpr41* in the mesenteric lymph node. *In vitro*, *B. longum* RAPO and its culture supernatant suppressed the expressions of pro-inflammatory cytokine genes in macrophages and inhibited myofibroblast differentiation in fibroblasts. These findings highlight the probiotic potential of *B. longum* RAPO in preventing tissue fibrosis by modulating macrophage activity and promoting the growth of SCFA-producing bacteria, underscoring the therapeutic potential of microbial modulation in SSc.


Keywords: Systemic sclerosis; Bacterial antibodies; *Bifidobacterium longum*; Fibrosis; Short-chain fatty acid


Juyeon Lee 
<https://orcid.org/0009-0000-8253-2614>

 Sang-Jun Park 
<https://orcid.org/0009-0000-0899-9670>


 Myeong Soo Park 
<https://orcid.org/0000-0003-4334-1457>


 Hanna Lee 
<https://orcid.org/0000-0002-2129-4269>


 Mingyo Kim 
<https://orcid.org/0000-0003-3744-8522>


 Yun-Hong Cheon 
<https://orcid.org/0000-0002-0099-6253>

 Seung-Geun Lee 
<https://orcid.org/0000-0002-5205-3978>

 Dong Hyun Sohn 
<https://orcid.org/0000-0002-9572-0611>

 Jae-Bum Jun 
<https://orcid.org/0000-0002-0208-0505>

 Suhee Kim 
<https://orcid.org/0000-0002-9315-0360>

 Sang-Il Lee 
<https://orcid.org/0000-0002-8283-7001>

Conflict of Interest

The authors declare no potential conflicts of interest.

Abbreviations

α-SMA, alpha smooth muscle actin; BAL, bronchoalveolar lavage; BLM, bleomycin; CCA, canonical correspondence analysis; CFU, colony-forming unit; CS, culture supernatant; dc, diffused cutaneous type; GNU, Gyeongsang National University; GNUH, Gyeongsang National University Hospital; GPCR, G protein-coupled receptor; HC, healthy controls; HK, heat-killed; hTGF-β1, human transforming growth factor-beta1; IPF-LF, lung fibroblast diagnosed with idiopathic pulmonary fibrosis; IHC, immunohistochemistry; LDA, linear discriminant analysis; LEfSe, linear discriminant analysis effect size; LF, lung fibroblast; MLN, mesenteric lymph node; NHDF, normal human dermal fibroblast; PCoA, principal coordinate analysis; SCFA, short-chain fatty acid; SSc, systemic sclerosis.

Author Contributions

Conceptualization: Hong ST, Lee SI; Data curation: Park HJ, Yu D, Lee J, Park SJ, Kim S; Formal analysis: Park HJ, Yu D, Hong ST, Park SJ, Kim S; Funding acquisition: Kim S, Lee SI; Investigation: Park HJ, Lee SG, Sohn DH, Jun JB, Kim, S; Methodology: Hong ST, Park MS, Lee SI; Project administration: Lee SI; Resources: Hong ST, Park MS, Lee H, Kim M, Cheon YH, Lee SG, Sohn DH, Jun JB;

INTRODUCTION

Systemic sclerosis (SSc) is a complex autoimmune disease affecting multiple organs, characterized by vascular injury, immune dysregulation, and fibrosis (1,2). Despite extensive research on the genetic, environmental, and immunological aspects, the exact etiology of SSc remains unclear, and effective treatments are still lacking (3,4). Therefore, elucidating the underlying mechanisms would aid in further developing targeted and efficacious therapies in SSc.

Gut microbiota potentially contributes to the development of SSc (5). Individuals with SSc often exhibit significant gastrointestinal tract involvement, with marked alterations in gut microbial composition, including an overrepresentation of pathogenic bacteria and a reduction in commensal bacteria (6). Moreover, changes in the gut microbiota, such as the reduced abundance of butyrate-producing bacteria and proliferation of Th17-activating bacteria, suggest the potential of microbiome-driven inflammation in SSc pathogenesis (7).

Animal studies have further supported the link between the gut microbiome and SSc pathologies, demonstrating that gut microbial dysbiosis in early-life aggravates fibrosis in SSc mice, while administering bacterial metabolites, such as sodium butyrate, ameliorates SSc-associated skin and lung fibrosis in mice (8,9). Although the precise mechanisms underpinning the microbiota-SSc connection are not fully elucidated, it is hypothesized that alterations in the gut microbiota may trigger immune dysregulation, contributing to the onset of SSc (10). Furthermore, probiotics containing *Bifidobacterium* and *Lactobacillus* species have shown promising immunomodulatory effects in patients with SSc, suggesting their potential therapeutic value (11). These findings offer a rationale for exploring microbiome-targeted interventions in SSc (12).

Recent research has highlighted the importance of identifying disease-specific microbes at the species or even strain levels for successful microbiome-targeted therapies (5), considering the divergent effects observed among bacteria within the same genus (13,14). However, traditional genomic approaches for gut microbiome profiling may have limited taxonomic resolution, particularly for identifying species or lower taxa (15). In contrast, immunology-based microarrays can offer a sensitive and efficient alternative, enabling the identification and differentiation of bacterial species or strains with simultaneous analysis of numerous interactions using minimal sample volumes (16). Several studies have demonstrated the efficacy of detecting serum Abs responsive to bacterial species (17,18), since bacterial cell surface antigens interact with the host immune system, eliciting Ab production (19). Distinct bacterial surface components can act as markers even among bacterial strains with similar cell surface architectures due to significant structural variations (20). Detecting bacteria-specific Ab responses is a promising approach for profiling targeted bacterial species in limited and extensive human serum samples.

Therefore, this study aimed to identify SSc-associated microbial species using a serum-based microbial microarray, explore potential microbial therapeutic candidates, and elucidate the underlying mechanisms of microbiome-mediated treatment in SSc. This research would provide valuable insights regarding involvement of the gut microbiota in SSc and facilitate the development of effective microbiome-targeted therapies.

Supervision: Lee SI; Validation: Hong ST, Park MS, Kim S, Lee SI; Visualization: Park HJ, Park SJ, Kim S; Writing - original draft preparation: Park HJ, Park SJ, Kim S; Writing - review & editing: Hong ST, Park MS, Kim S, Lee SI.

MATERIALS AND METHODS

Patients

This study included 76 patients diagnosed with SSc and 50 healthy controls (HC). Serum samples were obtained from Pusan National, Hanyang, and Gyeongsang National University Hospital (GNUH)-Korea Biobank in Korea between 2014 and 2018. This study was approved by the Institutional Review Board of GNUH (No. GNUH 2014-02-013).

Microbial microarray analysis

IgM levels against specific intestinal microbes were evaluated using a previously described method (21). Briefly, lysates of 384 intestinal microbial species were spotted onto a nylon membrane using a microarray spotter (CapitalBio, Beijing, China) and incubated with serum samples, followed by treatment with Alexa Fluor 647-conjugated goat anti-human IgM secondary Ab (Thermo Fisher Scientific, Waltham, MA, USA). Fluorescence intensity, indicating IgM levels, was quantified using Luxscan (CapitalBio). Richness, evenness, and compositional diversity were assessed. Linear discriminant analysis (LDA) effect size (LEfSe) and heatmap visualization were utilized to identify Abs against differentially enriched taxa ($p < 0.05$, LDA score > 3.0) and microbial species ($p < 0.01$, Z-ratio > 1.5), respectively. Canonical correspondence analysis (CCA) was conducted to investigate potential relationships between significantly different antimicrobial Abs and clinical parameters in patients with SSc.

Induction of SSc in mice and treatment with *Bifidobacterial* strains

Six-week-old male C57BL/6 mice (Koatech, Seoul, Korea) were acclimatized for 2 wk before initiating the experiments. Mice were randomly assigned to the following 3 experimental groups: 1) PBS-treated control (normal), 2) Bleomycin (BLM)-induced SSc (BLM), 3) *Bifidobacterium*-treated SSc (BLM/*Bifidobacterium*). SSc was induced following a previously described protocol (9). Briefly, mice received subcutaneous injections of 100 μ g BLM (Dong-A ST, Seoul, Korea) at a single dorsal location, 5 times a week for 2 wk. The *Bifidobacterium* strains used in this study were *Bifidobacterium longum* BORI, *B. longum* RAPO, and *B. bifidum* BGN4, provided by BIFIDO Co., Ltd., Hongcheon, Korea. Live *Bifidobacterium* strains were orally administered at a dose of approximately $1\text{--}5 \times 10^9$ colony-forming units (CFUs) per mouse, 5 times a week for 4 wk, beginning 2 wk before BLM injections. All animal experiments were conducted in accordance with the guidelines of Gyeongsang National University (GNU) and approved by the Institutional Animal Care and Use Committee in Korea (approval ID: GNU-221212-M0179).

Histological examination

Formalin-fixed, paraffin-embedded skin and lung sections (5 μ m) from mice were stained with Masson's trichrome and examined under a Nikon Eclipse Ni-U microscope (Nikon Instruments, Tokyo, Japan). Dermal thickness was measured at 6 sites within each skin section to assess skin fibrosis. Fibrotic changes in lung tissues were evaluated using the Ashcroft score (22), along with collagen and alveolar area percentages at 9 sites. Scores were averaged from multiple sites.

Immunofluorescence and immunohistochemistry (IHC) staining

Skin and lung tissue sections were deparaffinized before staining. For immunofluorescence, sections were incubated for 16 h with primary Abs against alpha smooth muscle actin (α -SMA, Abcam, Cambridge, UK), CD11b (Santa Cruz Biotechnology, Dallas, TX, USA), and CX3CR1 (Santa Cruz Biotechnology) at 4°C, followed by treatment with a fluorescence-conjugated secondary Ab (anti-mouse Alexa Fluor 488, anti-rat Alexa Fluor 488, or anti-

mouse Alexa Fluor 594, Thermo Fisher Scientific) at 20°C–25°C for 2 h. Slides were mounted using an antifade reagent containing DAPI (Thermo Fisher Scientific).

For IHC, sections were stained using a VECTASTAIN Elite ABC Peroxidase Kit (Vector Laboratories, Burlingame, CA, USA). α -SMA Ab (Abcam) was applied, followed by incubation with a biotinylated secondary Ab (Vector Laboratories), and color development using the 3,3'-diaminobenzidine systems (Sigma-Aldrich, St. Louis, MO, USA). Images were captured using a Nikon microscope imaging system at 400 \times magnification. Quantification of fluorescent signals and α -SMA positivity was performed using the ImageJ software (National Institutes of Health, Bethesda, MD, USA).

Digital polymerase chain reaction

B. longum and its strain RAPO were quantified using the QIAcuity digital PCR system (Qiagen, Hilden, Germany) following the manufacturer's instructions. Briefly, total bacterial genomic DNA was extracted from mice fecal samples using the MagMAX™ Microbiome Ultra Nucleic Acid Isolation Kit (Thermo Fisher Scientific). Reaction mixtures, containing QIAcuity Probe Master Mix (Qiagen), primer/probe mix (**Supplementary Table 1**), and template DNA, were transferred to QIAcuity Nanoplate 96-well (Qiagen). The nanoplate was then loaded onto the QIAcuity One 5plex system (Qiagen) for automated partitioning and PCR amplification (95°C for 2 min, followed by 50 cycles of 95°C for 15 s and 60°C for 30 s). After thermocycling, fluorescence from each well was analyzed using QIAcuity Software Suite (Qiagen).

Western blot analysis

Tissue and cell proteins were extracted, and western blotting for α -SMA was processed as previously described (9). Signal quantification was performed using Image Lab software (Bio-Rad, Hercules, CA, USA), normalized to β -actin.

Cell isolation and flow cytometric analysis

Bronchoalveolar lavage (BAL) fluid, mesenteric lymph node (MLN), and spleen cells were obtained from mice according to a previously described protocol (9). Subsequently, cells were stained with fluorochrome-conjugated Abs (**Supplementary Table 2**) and analyzed using an LSRFortessa™ X-20 flow cytometer (BD Biosciences, San Jose, CA, USA). FlowJo software (Tree Star Inc., Ashland, OR, USA) was used for further data analysis.

Differential cell counts and measurements of total protein and cytokine concentrations in BAL fluid

Slides were prepared by cytocentrifugation of BAL cells and stained with Diff-Quik (BioGnost, Zagreb, Croatia). Differential cell counts of leukocyte subsets were determined by examining a minimum of 300 cells per slide under a light microscope. The total protein concentration of BAL fluid was determined using the Bradford assay (Bio-Rad). Levels of IL-6, TNF- α , and IL-1 β in the BAL fluid were measured using DuoSet ELISA kits (R&D System, Minneapolis, MN, USA), following the manufacturer's instructions.

Cytokine production of MLN and spleen cells

MLN and spleen cells isolated from experimental mouse groups were seeded into a 96-well plate at a density of 5 \times 10⁵ cells per well. The cells were stimulated with 1 μ g/ml of LPS (Sigma-Aldrich) at 37°C with 5% CO₂. After 16 h, the supernatants were collected and the levels of IL-6 and TNF- α were measured. IL-10 levels were measured in the supernatants collected after 40 h using the OptEIA™ Mouse IL-10 ELISA Set (BD Biosciences).

Quantitative real-time PCR

Total RNA extraction and subsequent quantitative real-time PCR were conducted as previously described (9). Relative expression levels of target genes were determined using the $2^{-\Delta\Delta Ct}$ comparative method, normalized to GAPDH. Details on TaqMan assays and SYBR primers can be found in **Supplementary Table 3**.

16S rRNA gene sequencing and analysis

Bacterial genomic DNA was extracted from mouse fecal samples, and sequencing was conducted as previously described (21). Raw sequence reads were analyzed using QIIME2 software. All amplicon sequence variants were classified using the SILVA 138 99% database. Microbial richness, evenness diversity indices, and principal coordinate analysis (PCoA) were performed using the QIIME2 pipeline and R software (R Foundation for Statistical Computing, Vienna, Austria). All sequencing raw data are available at the NCBI Sequence Read Archive repository, accession number, PRJNA1108506 (<https://www.ncbi.nlm.nih.gov/bioproject/PRJNA1108506>).

Short-chain fatty acid (SCFA) analysis

The concentration of SCFAs in mouse fecal samples was measured using gas chromatography/mass spectrometry (GC-2010 Plus, GCMS-TQ 8030, Shimadzu, Tokyo, Japan).

Cell culture and treatment

The murine macrophage cell line RAW 264.7 (1×10^5 cells/well) was cultured for 24 h in a 24-well plate using DMEM, supplemented with 10% fetal bovine serum, 100 U/ml penicillin, and 100 mg/ml streptomycin (Gibco, Carlsbad, CA, USA) at 37°C with 5% CO₂. The cells were then co-cultured with different doses of heat-killed (HK)-*B. longum* RAPO (multiplicity of infection: 0, 0.1, or 1) or cell-free culture supernatant (CS) derived from live *B. longum* RAPO (final concentrations of 0, 0.01, or 0.1%) for 20 h, followed by stimulation with 1 µg/ml LPS for 4 h. Detailed information on HK-bacteria and CS preparation is provided in **Supplementary Data 1**.

Primary normal human dermal fibroblasts (NHDFs, ATCC, Gaithersburg, MD, USA) were seeded in a 6-well plate (2×10^5 cells/well) using DMEM with supplements. After 24 h of culture, NHDFs were treated with 10 ng/ml of human TGF-β1 (hTGF-β1, R&D System) with or without *B. longum* RAPO CS (2%) for 48 and 72 h.

Normal lung fibroblasts (normal-LFs, LL24, ATCC) and LFs diagnosed with idiopathic pulmonary fibrosis (IPF-LFs, LL29, ATCC) were cultured in Ham's F-12 medium (Gibco) with supplements. The fibroblasts were stimulated with 5 ng/ml of hTGF-β1 with or without *B. longum* RAPO CS (2%) for 72 h.

Statistical analyses

Data analysis and visualization were conducted using IBM SPSS (Chicago, IL, USA) or GraphPad Prism (San Diego, CA, USA). Statistical significance was assessed using analysis of variance or Kruskal-Wallis test, followed by *post hoc* tests. Permutational multivariate analysis of variance was used to evaluate differences in the microbial community. Results are presented as mean ± SD unless otherwise specified, and $p < 0.05$ was considered significant.

RESULTS

Alterations in serum antimicrobial Ab levels in patients with SSc

Our study involved the use of a serum-based bacterial microarray to investigate microbial alterations and identify potential therapeutic bacterial targets specific to SSc. Serum samples from patients with SSc and HC were analyzed for IgM Ab levels against 384 gut microbial species. Detailed patient characteristics are summarized in **Supplementary Table 4**. Although no significant differences were observed in the α -diversity of serum antimicrobial Abs (**Fig. 1A**), the β -diversity clustering pattern differed considerably between patients with SSc and HC (**Fig. 1B**). Through LEfSe analysis, we identified core antimicrobial Abs distinguishing patients with SSc from HC, including enrichment in anti-Actinobacteria and anti-Bacteroidetes Abs in HC and anti-Proteobacteria Abs in patients with SSc at the phylum level (**Fig. 1C**). At lower taxonomic levels, HC exhibited enriched antimicrobial Abs in classes Actinobacteria, Coriobacteriia, and Bacteroidia, as well as orders Bifidobacteriales, Corynebacteriales, Coriobacteriales, Bacteroidales, and Bacillales, spanning 4 families and 4 genera. Conversely, patients with SSc demonstrated enrichment in antimicrobial Abs against classes Clostridia and Tissierellia, encompassing 4 orders, 4 families, and one genus.

Our investigation revealed 28 significantly altered antimicrobial Abs at the species level in patients with SSc, compared to those in HC, among which 12 exhibited reduced levels and 16 displayed increased levels (**Fig. 1D**). Using CCA and Pearson correlation analysis, we found potential associations between specific antimicrobial Abs and clinical phenotypes of SSc (**Fig. 1E**, **Supplementary Table 5**). Notably, Abs against *Corynebacterium diphtheriae*, *Enorma timonensis*, *Escherichia vulneris*, *Citrobacter werkmanii*, *Pseudomonas fluorescens*, and *Lactobacillus animalis* correlated with the presence of autoantibodies in patients with SSc (**Fig. 1E**). Particularly, anti-*C. diphtheriae*, anti-*P. fluorescens*, and anti-*L. animalis* Abs positively correlated with the presence of anti-Scl-70, while anti-*E. vulneris* and anti-*C. werkmanii* Abs correlated positively with anti-centromere autoantibody presence (**Supplementary Table 5**). Moreover, anti-*Bacillus thermoamylovorans* Ab correlated with cutaneous type and lung involvement in patients with SSc (**Fig. 1E**), with negative correlations observed with diffused cutaneous type (dc) and lung involvement (**Supplementary Table 5**).

Among the decreased serum antimicrobial Abs in patients with SSc, we focused on those targeting *Bifidobacterium adolescentis* and *B. longum*. These well-known probiotics are recognized for promoting the growth of butyrate-producing bacteria by supplying acetate as a substrate (23), potentially contributing to SSc suppression through butyrate formation (9). Remarkably, Ab levels against both these *Bifidobacterium* species were diminished in patients with SSc compared to those in HC, irrespective of the clinical phenotypes of SSc (**Fig. 1F**). Specifically, *B. longum* was the predominant probiotic species in HC compared to those in patients with SSc, as indicated by the LDA score (**Supplementary Fig. 1**). Subsequently, we comprehensively investigated the therapeutic potential of *B. longum* as a promising microbial target for treating SSc.

B. longum RAPO ameliorates dermal and lung fibrosis in BLM-induced SSc mice

To determine the therapeutic potential of *B. longum* in SSc, we explored the antifibrotic efficacy of the *B. longum* strains, BORI and RAPO, along with that of *B. bifidum* BGN4, in a BLM-induced murine SSc model. SSc was induced in mice by subcutaneous injections of 100 μ g BLM at the dorsal lesion site, administered 5 times a week for 2 wk. The *Bifidobacterium* strains were orally administered 5 times a week for 4 wk, starting 2 wk before BLM injections

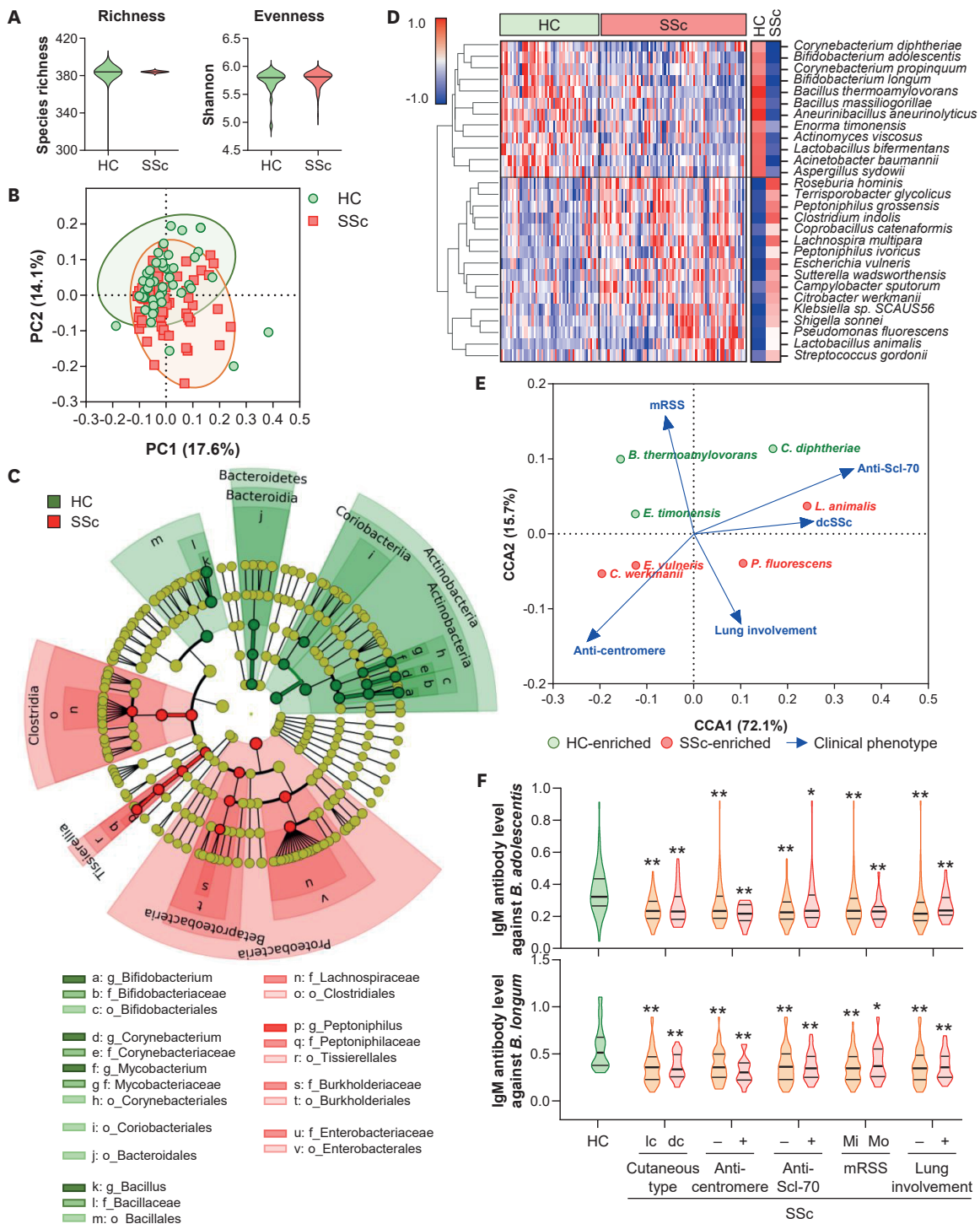


Figure 1. Comparison of serum antimicrobial Ab profile between HC (n=50) and patients with SSC (n=76). (A) Alpha-diversity assessment of antimicrobial Ab abundances (Mann-Whitney test). (B) PCoA plot based on Bray-Curtis dissimilarity of antimicrobial Ab communities (PERMANOVA, p<0.001). Each symbol represents an individual. (C) Cladogram generated using LefSe analysis. The phylogenetic tree shows taxa enriched in HC and SSc represented in green and red, respectively (pairwise Wilcoxon test, p<0.05, LDA score>3.0). (D) Heatmap illustrating differential antimicrobial Ab abundances between HC and patients with SSC (t- and z-tests, p<0.01, Z-ratio>1.5). Colors represent abundance levels, ranging from blue (low abundance) to red (high abundance). (E) CCA diagram visualizing the relationship between differential antimicrobial Abs (circles) and clinical phenotypes (arrows) in patients with SSC. (F) Comparative levels of significantly different antimicrobial Abs against *Bifidobacterium* species among HC and patients with SSC, stratified according to clinical phenotypes. Ic, limited cutaneous; Mi, Mild; Mo, Moderate; mRSS, Modified Rodnan skin score. One-way analysis of variance, Sidak *post hoc* test, **p<0.01 vs. HC.

(Fig. 2A). Among SSc mice orally administered *Bifidobacterium* strains at a dose of 2×10^9 CFUs per mouse, significant improvements in both dermal and lung fibrosis were exclusively observed in the *B. longum* RAPO-treated group (Fig. 2B-D). *B. longum* RAPO notably reduced dermal thickness (Fig. 2C) and attenuated lung fibrotic changes indicated by the Ashcroft score, collagen area, and alveolar area (Fig. 2D). The *B. longum* BORI-treated group partially ameliorated lung fibrosis, manifested by an increase in alveolar area (Fig. 2D). In an additional experimental study involving various doses of administered *Bifidobacterium* strains, 2×10^9 CFUs of *B. longum* RAPO effectively mitigated both dermal and lung fibrosis (Fig. 2E-G). Neither *B. longum* BORI nor *B. bifidum* BGN4 suppressed dermal fibrosis at the tested doses ranging from 1×10^9 to 5×10^9 CFUs (Supplementary Fig. 2).

Consistently reproducible suppression of BLM-induced dermal and lung fibrosis was observed with 2×10^9 CFUs of *B. longum* RAPO in independent *in vivo* experiments (Fig. 3A-C). Successful colonization of the administered *B. longum* RAPO in BLM mice was confirmed, demonstrating a notable elevation in the fecal levels of *B. longum* RAPO following its administration (Fig. 3D). Immunofluorescence and IHC staining revealed a marked reduction in the expression of α -SMA, a myofibroblast marker, in the skin and lung tissues of BLM mice following *B. longum* RAPO administration (Fig. 3E). Moreover, *B. longum* RAPO administration decreased α -SMA protein expression in the skin of BLM mice, although the observed effect on lung tissue was not significant (Fig. 3F). In summary, *B. longum* RAPO, particularly at a dose of 2×10^9 CFUs, effectively attenuated dermal and lung fibrosis in BLM-induced SSc mice by impeding structural fibrotic changes and myofibroblast differentiation.

***B. longum* RAPO inhibits pro-inflammatory macrophage infiltration into fibrotic lesions in BLM-induced SSc mice**

In our previous investigation, we noted significant macrophage infiltration in the fibrotic skin and lung tissues of SSc mice (9). To elucidate the mechanistic basis of *B. longum* RAPO's therapeutic efficacy in SSc, we examined macrophage populations in the skin and lungs of *B. longum* RAPO-treated versus untreated BLM mice (Fig. 4). Immunofluorescence analysis revealed a notable reduction in the percentage of CD11b⁺CX3CR1⁺ macrophage areas in the skin of BLM mice treated with *B. longum* RAPO (Fig. 4A). Morphological evaluation of BAL cells revealed that macrophages were the predominant cell type in the BAL fluid of BLM mice, exhibiting an activated phenotype characterized by enlarged and vacuolated cytoplasm, which was alleviated by *B. longum* RAPO treatment (Fig. 4B). Furthermore, *B. longum* RAPO effectively diminished the infiltration of total immune cells, particularly macrophages, in the BAL fluid of BLM mice.

Flow cytometric analysis of BAL cells (Supplementary Fig. 3), demonstrated a significant reduction in the number of total macrophages (CD45⁺CD64⁺), particularly alveolar macrophage (CD45⁺CD64⁺CD11c⁺CD11b⁻), in *B. longum* RAPO-treated BLM mice compared to that in untreated BLM mice (Fig. 4C). Moreover, *B. longum* RAPO administration decreased the accumulation of inflammatory components, such as total protein and IL-6, in BAL fluid of BLM mice (Fig. 4D and E). Gene expression analysis revealed the downregulation of profibrotic (*Acta2*, *Ctgf*, and *Tgfb1*) and pro-inflammatory cytokines (*Il6*, *Il1b*, and *Tnfa*) and monocyte/macrophage chemoattractant (*Ccl2*) genes in the skin and lungs of *B. longum* RAPO-treated BLM mice (Fig. 4F, Supplementary Fig. 4). In summary, *B. longum* RAPO treatment not only reduced macrophage recruitment to the skin and lungs but also inhibited macrophage activation and tissue inflammation within the fibrotic tissues in BLM-induced SSc mice.

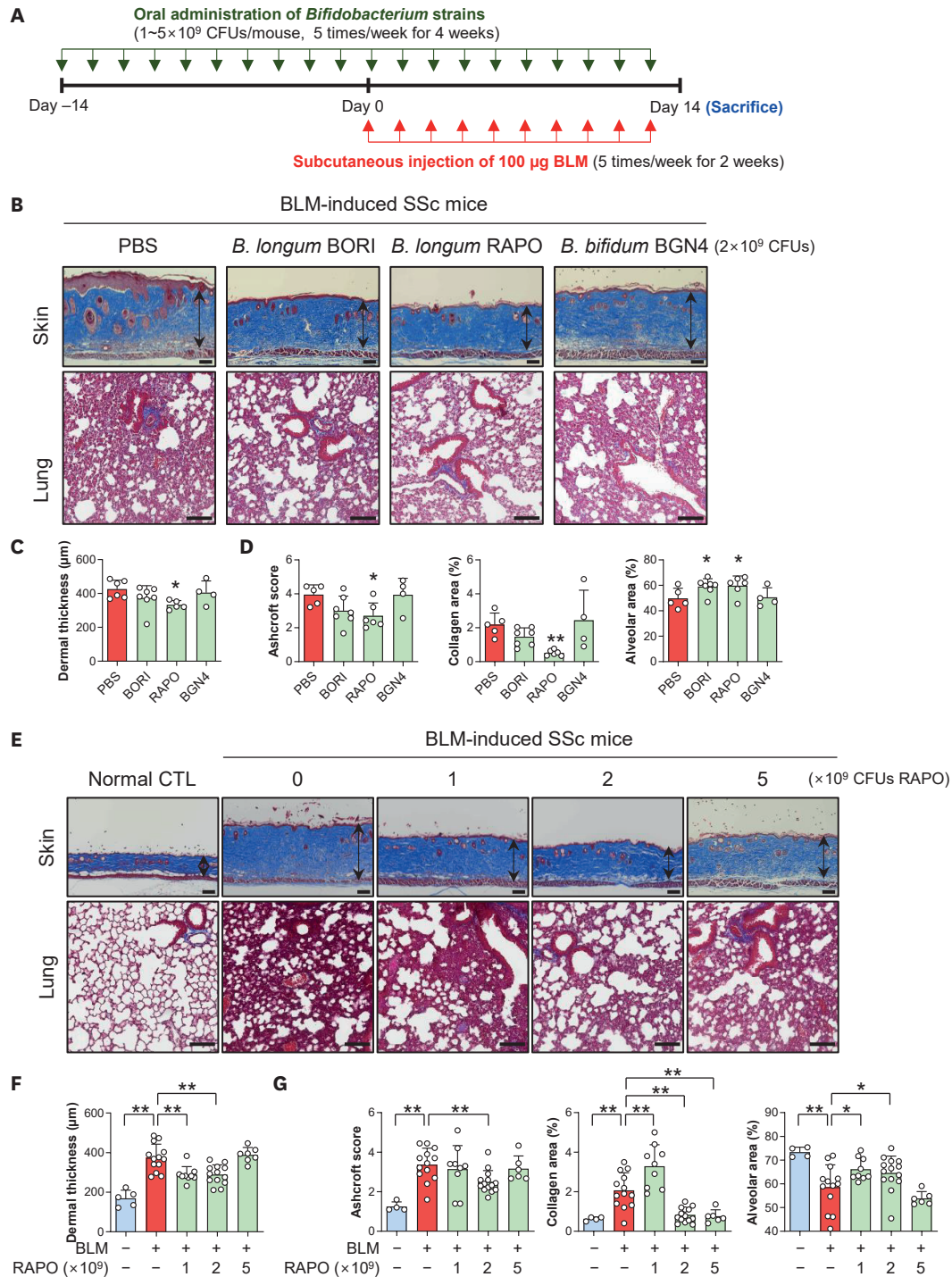


Figure 2. Effects of *Bifidobacterium* strains on dermal and lung fibrosis in BLM-induced SSc mice. (A) Experimental scheme: SSc was induced in mice through subcutaneous injections of BLM to the dorsal skin, 5 times per week for 2 wk. Oral administration of *Bifidobacterium* strains commenced 2 wk before BLM injection and continued for the subsequent 4 wk. Skin and lung tissues were then obtained from mice in each experimental group to evaluate fibrosis. (B–D) Representative images of Masson's trichrome stain illustrating skin and lung fibrosis (B), evaluation of skin fibrosis by dermal thickness (C), and assessment of lung fibrosis using the Ashcroft score and the percentages of collagen and alveolar area (D) in skin and lung tissues obtained from SSc mice treated with PBS (n=6), *Bifidobacterium longum* BORI (n=7), *B. longum* RAPO (n=6), or *B. bifidum* BGN4 (n=4). Arrow length indicates dermal thickness in skin tissues. *p<0.05, **p<0.01 vs. PBS. (E–G) Representative images of Masson's trichrome stain (E) and evaluation of skin (F) and lung fibrosis (G) in skin and lung tissues obtained from normal (n=5) and SSc mice treated with *B. longum* RAPO at doses of 0 (n=13), 1 (n=9), 2 (n=14), or 5 × 10⁹ CFUs (n=7). *p<0.05, **p<0.01. Scale bars=100 μm. Mean ± SD.

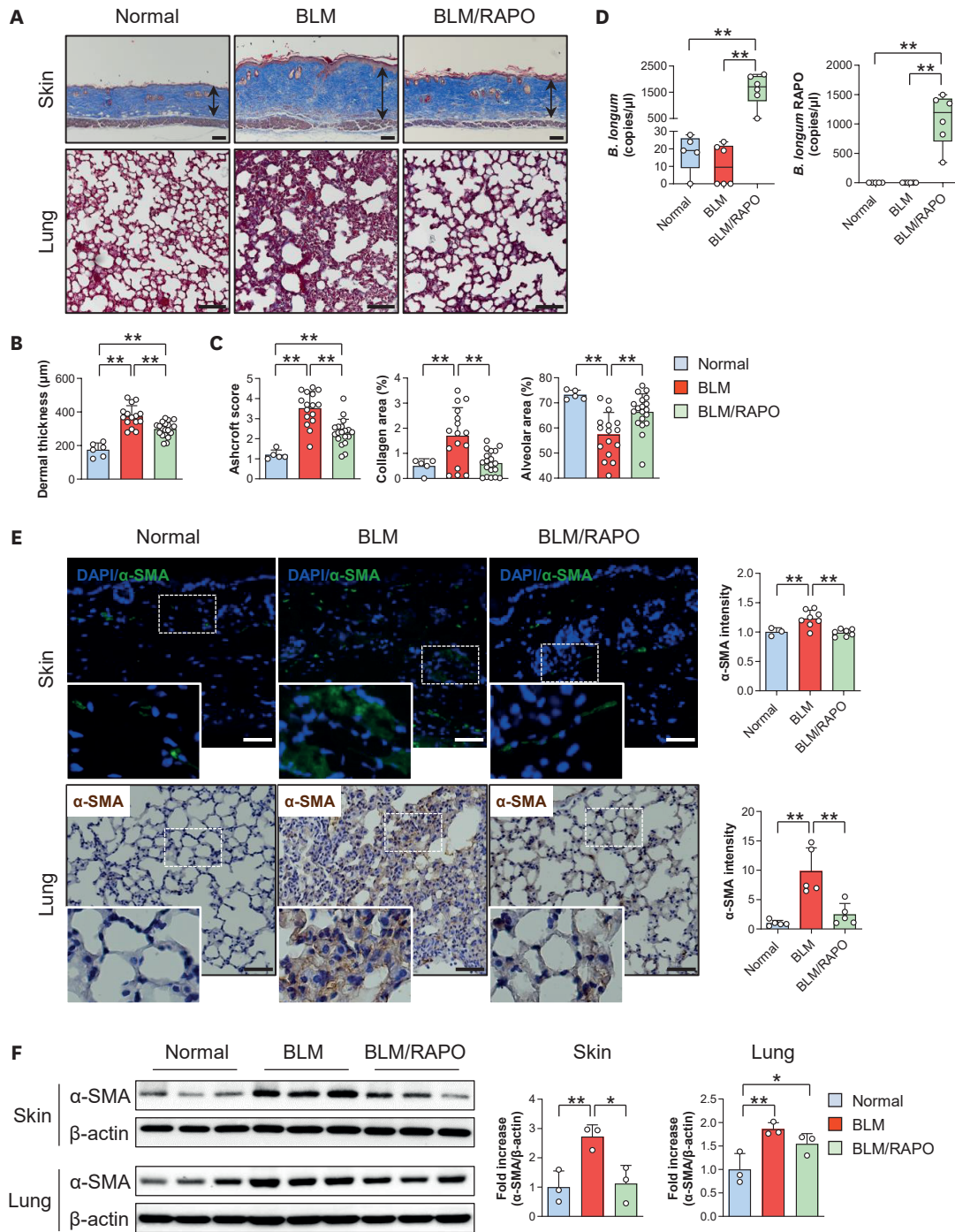


Figure 3. Antifibrotic effects of *B. longum* RAPO on dermal and lung fibrosis in BLM-induced SSc mice. SSc was induced in mice through subcutaneous injections of BLM to the dorsal skin for 2 wk. Oral administration of *B. longum* RAPO, at a dose of 2×10^9 CFUs, commenced 2 wk before BLM injection and continued for 4 wk. Skin, lung, and fecal samples were then obtained from mice in each experimental group. (A–C) Representative images of Masson’s trichrome stain showing skin and lung fibrosis (A), accompanied by quantitative analysis of fibrosis in skin (B) and lung tissues (C) obtained from mice of normal (n=6), BLM (n=16), and BLM/RAPO (n=19) groups. Scale bars=100 μm . (D) Quantification of *B. longum* and its strain RAPO in fecal samples using digital PCR (n=5–6/group). (E) Representative images of immunofluorescence (green) and IHC (brown) staining for α -SMA in skin and lung tissues, respectively, and quantification of α -SMA expression (n=3–5 for normal, 5–8 for BLM, and 5–7 for BLM/RAPO group). Scale bars=50 μm . (F) Expression of α -SMA protein in skin and lung tissues (n=3/group). Mean \pm SD, *p<0.05, **p<0.01.

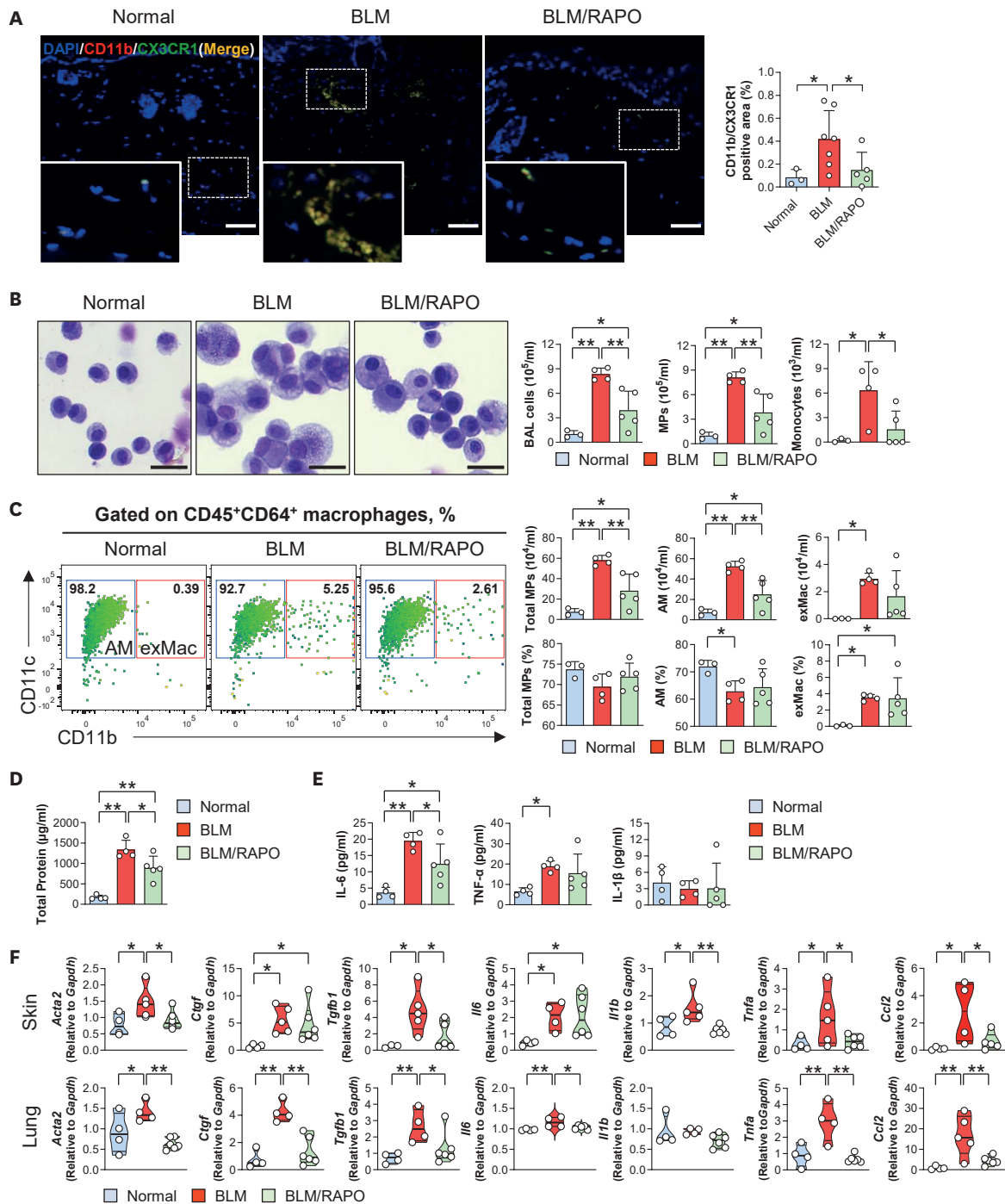


Figure 4. Anti-inflammatory effects of *B. longum* RAPO on dermal and lung fibrosis in BLM-induced SSC mice. SSC was induced in mice through subcutaneous injections of BLM to the dorsal skin for 2 wk. Oral administration of *B. longum* RAPO commenced 2 wk before BLM injection and continued for 4 wk. Skin, lung, and BAL fluid were then obtained from mice of normal (n=3-4), BLM (n=4-7), and BLM/RAPO (n=5-6) groups. (A) Immunofluorescent images and quantification showing expression of CD11b⁺CX3CR1⁺ macrophages in skin tissues stained for DAPI (blue), CD11b (green), and CX3CR1 (red). Scale bars=50 μ m. (B) Differential cell counts of BAL cells stained with Diff-Quik. Scale bars=25 μ m. (C) Flow cytometric analysis of macrophage populations in BAL cells. Total macrophages (MPs, CD45⁺CD64⁺) were assessed, and macrophage subsets were further divided into alveolar macrophages (CD11c⁺CD11b⁻) and exudate macrophages (exMac, CD11c⁺CD11b⁺). (D, E) Quantification of total protein (D) and pro-inflammatory cytokine concentrations in BAL fluid (E). (F) Expression of genes for profibrotic and pro-inflammatory cytokines and chemokine in the skin and lung tissues. Mean \pm SD, *p<0.05, **p<0.01.

B. longum RAPO modulates inflammatory monocyte recruitment and immune response in the lymphoid organs of BLM-induced SSc mice

In addition to macrophage infiltration observed in fibrotic skin and lung tissues, our previous study identified inflammatory monocyte recruitment to the MLN and spleen in SSc mice (9). This recruitment represents a critical early inflammatory event, followed by their differentiation into activated macrophages and subsequent downstream inflammatory responses (24).

Considering the potential pathological mechanisms underlying SSc, we investigated the modulatory effect of *B. longum* RAPO on inflammatory monocyte recruitment to lymphoid organs. Our analysis revealed a significant inhibition of Ly6C⁺ inflammatory monocyte recruitment to the spleen in *B. longum* RAPO-treated BLM mice compared to that in untreated BLM mice, while no differences were observed in MLN between the 2 groups (Fig. 5A).

To further elucidate *B. longum* RAPO's mechanism in suppressing fibrosis, we assessed the cytokine and chemokine gene expressions of MLN and spleen cells isolated from mice (Fig. 5B, Supplementary Fig. 4). We found upregulated *Ccl2* expression, crucial for Ly6C^{hi} monocyte migration and macrophage activation, in MLN and spleen cells of BLM mice. This upregulation was significantly suppressed in both MLN and spleen cells of *B. longum* RAPO-treated BLM mice (Fig. 5B). Moreover, we noted reduced TNF- α production in the MLN cells of *B. longum* RAPO-treated BLM mice, while IL-10 production was enhanced in both MLN and spleen cells of *B. longum* RAPO-treated BLM mice compared to that in untreated BLM mice (Fig. 5C). In conclusion, the inhibitory effect of *B. longum* RAPO on fibrosis may be attributed to its ability to suppress inflammatory monocyte recruitment to the spleen via *Ccl2* downregulation and its anti-inflammatory action in gut-draining MLN.

B. longum RAPO improves gut microbial diversity and enhances the expansion of SCFA-producing bacteria in BLM-induced SSc mice

To explore the impact of *B. longum* RAPO on gut microbiota modulation in SSc, we performed 16S rRNA gene sequencing analysis on fecal samples from experimental mice. Alpha-diversity analysis showed that *B. longum* RAPO treatment tended to restore both the richness and evenness of the gut microbial community disrupted in BLM-induced SSc mice (Fig. 6A). Specifically, significant enhancement in gut microbial evenness, as indicated by the Shannon index, was observed in *B. longum* RAPO-treated BLM mice compared to that in untreated BLM mice. Considerable differences were observed in the microbial composition among the experimental groups, as illustrated by significant differences in the overall fecal microbial community composition shown in PCoA plots (Fig. 6B).

At the phylum level, Firmicutes, Actinobacteria, and Patescibacteria were predominant in normal, untreated BLM, and *B. longum* RAPO-treated BLM mice, respectively (Fig. 6C). Noteworthy changes at the genus level, particularly in SCFA-producing genera, were observed between groups, as depicted in a heatmap (Fig. 6D). Fecal samples from normal and *B. longum* RAPO-treated BLM mice were notably abundant in SCFA-producing genera, including *Lachnospiraceae* NK4A136 group, *Roseburia*, *Lachnospiraceae* ASF356, *Oscillospiraceae*, *Lachnospiraceae*, *Eubacterium ruminantium* group, *Ruminococcaceae* Incertae Sedis, *Coriobacteriaceae* UCG-002, *Allobaculum*, *Prevotellaceae* Ga6A1 group, *Prevotellaceae*, *Candidatus Saccharimonas*, *Prevotellaceae* NK3B31 group, and *Clostridia* UCG-014 (Fig. 6D, Supplementary Fig. 5).

To further elucidate the potential mechanism underlying *B. longum* RAPO's mitigation of skin and lung fibrosis through SCFA production, we measured the levels of SCFAs, including

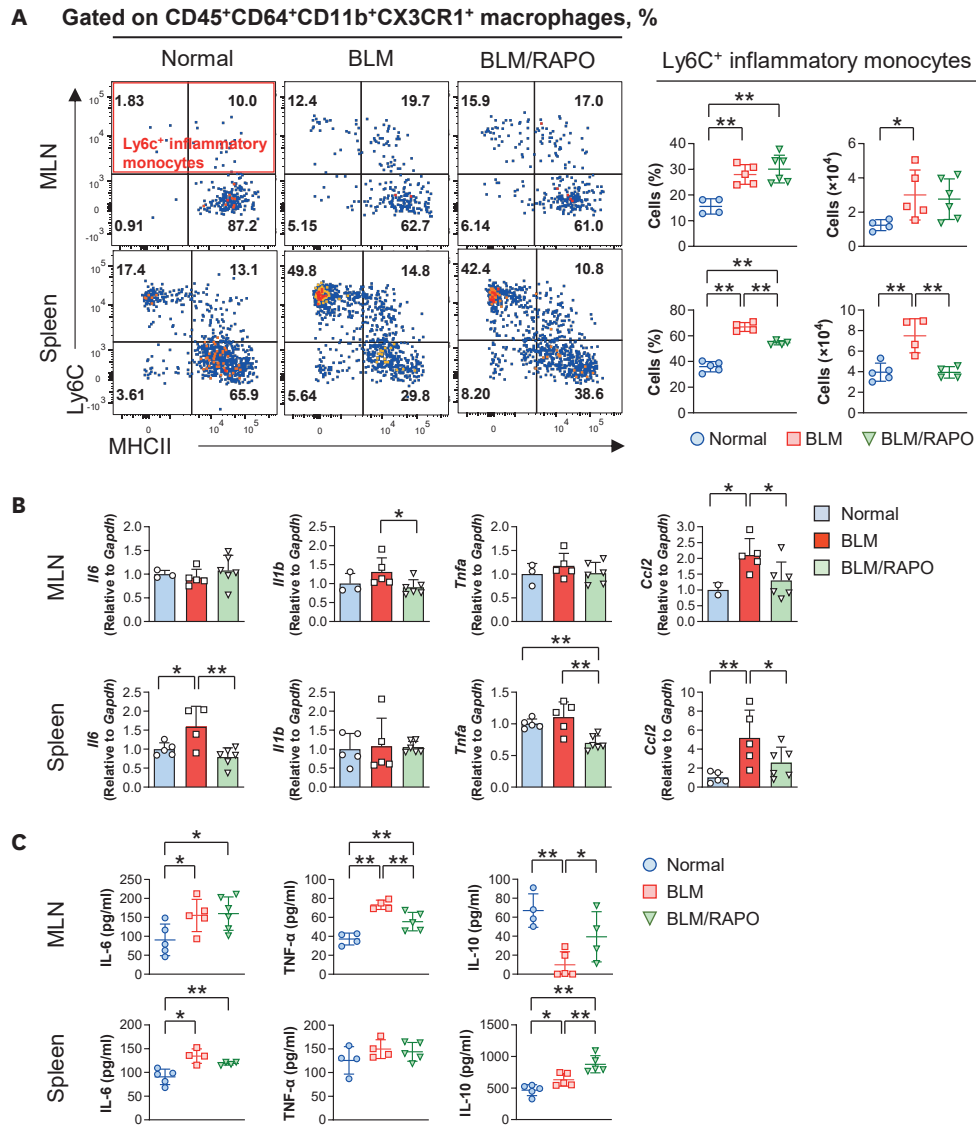


Figure 5. Immunomodulatory impacts of *B. longum* RAPO on the MLNs and spleen in BLM-induced SSc mice. Mice were subjected to subcutaneous injections of BLM to the dorsal skin for 2 wk and treated with or without *B. longum* RAPO 2 wk before BLM injection. Cells from MLN and spleen were isolated from normal (n=3–4), BLM-treated (n=4–5), and BLM/RAPO-treated (n=4–6) mice. (A) Flow cytometric analysis characterized macrophage populations in MLN and spleen cells. The numbers and percentages of Ly6C⁺ inflammatory monocytes, including newly recruited (Ly6C⁺MHCII⁻) and maturing monocytes (Ly6C⁺MHCII⁺), were assessed among total macrophages (CD45⁺CD64⁺CD11b⁺CX3CR1⁺). (B) Expression levels of pro-inflammatory cytokines and chemokine genes in MLN and spleen cells. (C) Immune responses of MLN and spleen cells. Cytokine levels secreted upon stimulation with LPS were measured in CSs from MLN and spleen cells. Mean \pm SD, *p<0.05, **p<0.01.

acetate, propionate, and butyrate, in fecal samples and examined the activation of SCFA-sensing G protein-coupled receptors (GPCRs) in MLN cells. Our results demonstrated a significant increase in fecal butyrate levels in *B. longum* RAPO-treated BLM mice compared to untreated BLM mice (Fig. 6E), along with upregulation of *Gpr41* expression in the MLN cells from *B. longum* RAPO-treated BLM mice relative to untreated normal and BLM mice (Fig. 6F, Supplementary Fig. 6). These findings suggest that butyrate-mediated *Gpr41* activation plays a pivotal role in the therapeutic efficacy of *B. longum* RAPO in the SSc mouse model. In summary, *B. longum* RAPO treatment effectively restores fecal microbial diversity, enhances the abundance of SCFA-producing gut bacteria, increases fecal butyrate production, and

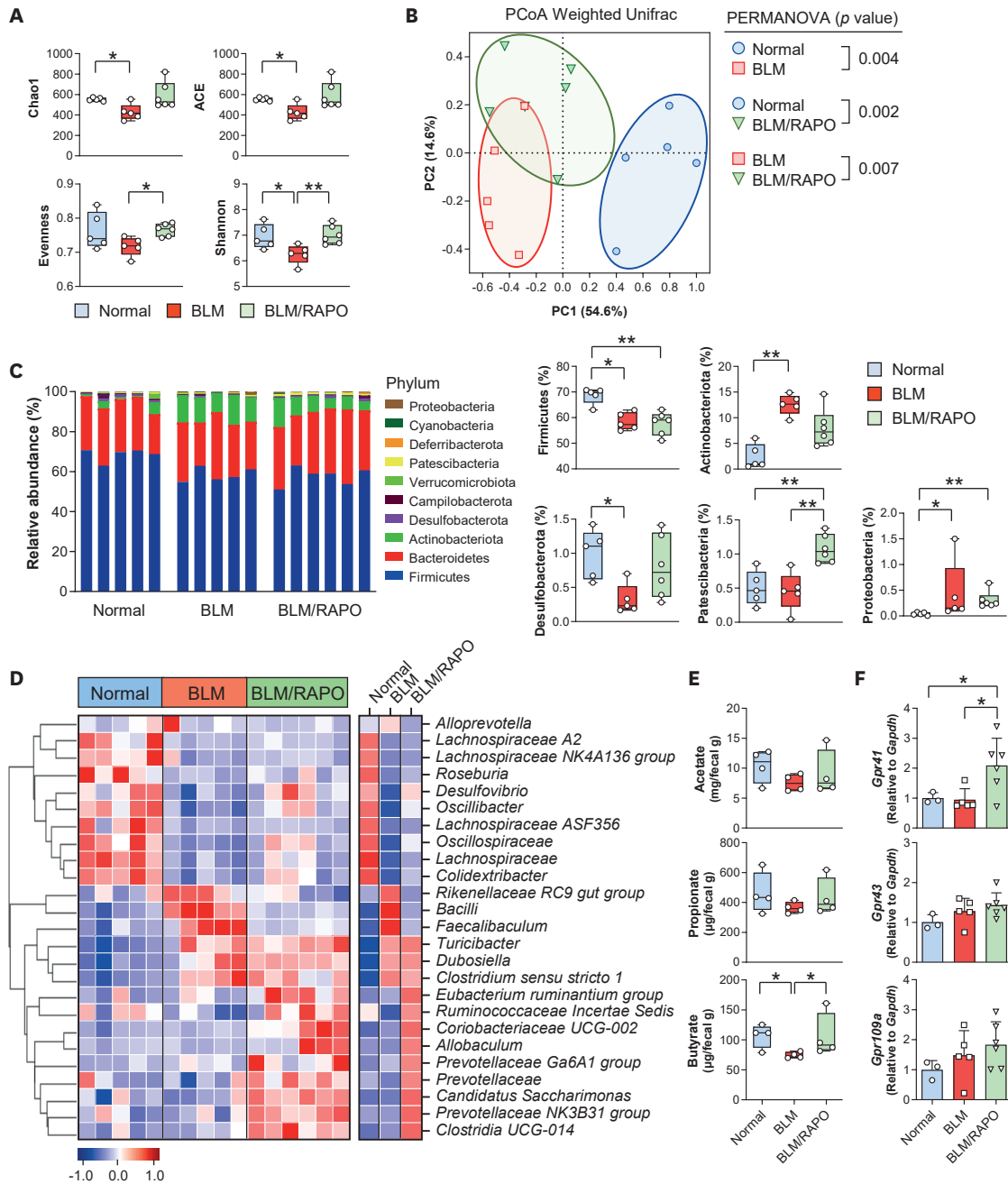


Figure 6. Influences of *B. longum* RAPO on gut microbiota in BLM-induced SSc mice. Mice were subjected to subcutaneous injections of BLM to the dorsal skin for 2 wk and treated with or without *B. longum* RAPO 2 wk before BLM injection. Fecal samples were collected from normal (n=5), BLM-treated (n=5), and BLM/RAPO-treated (n=6) mice, and 16S rRNA gene sequencing was conducted. (A) Alpha-diversity analysis of gut microbiota. (B) Beta-diversity assessed using PCoA based on Weighted UniFrac distance matrix. (C) Relative abundances of gut microbiota at the phylum level. (D) Heatmap illustrating significantly differential genera between groups (p<0.05). Colors represent abundance levels, ranging from blue (low abundance) to red (high abundance). (E) Measurement of SCFA levels in fecal samples from normal, BLM-treated, and BLM/RAPO-treated mice (n=4/group). (F) Expression levels of GPCR genes in MLN cells isolated from normal (n=3), BLM-treated (n=5), and BLM/RAPO-treated (n=6) mice, as determined using quantitative PCR. Mean ± SD, *p<0.05, **p<0.01.

activates the SCFA receptor *Gpr41* in gut-draining lymphoid cells, thereby potentially exerting a suppressive effect on the disease.

B. longum RAPO and its CS suppress the expression of pro-inflammatory and profibrotic mediators in macrophages and fibroblasts

To investigate the direct modulation of macrophage activation by *B. longum* RAPO, its secreted components, or metabolites under inflammatory conditions, we assessed pro-inflammatory gene expression induced by LPS in RAW 264.7 macrophages cultured with or without HK-*B. longum* RAPO or its CS. Doses of HK-*B. longum* RAPO or its CS were determined based on cytotoxicity evaluation (**Supplementary Fig. 7A**). Both the samples treated with HK-*B. longum* RAPO and its CS exhibited significant dose-dependent downregulation of LPS-induced genes, including *Il6*, *Il1b*, *Tnfa*, and *Ccl2* in RAW 264.7 cells (**Fig. 7A**).

To further explore the potential anti-fibrotic mechanism of *B. longum* RAPO mediated by soluble molecules, we evaluated the trans-differentiation of fibroblasts into myofibroblasts induced by hTGF- β 1 while treating dermal and LFs with or without of *B. longum* RAPO CS. The concentrations of *B. longum* RAPO CS were selected based on cytotoxicity evaluation (**Supplementary Fig. 7B**). *B. longum* RAPO CS effectively inhibited hTGF- β 1-induced myofibroblast transition in NHDFs, as evidenced by reduced α -SMA protein expression (**Fig. 7B**). Consistently, *B. longum* RAPO CS suppressed the expression of profibrotic genes such as *ACTA2* and *CTGF*, as well as pro-inflammatory genes including *IL6* and *IL1B*, during co-culture with NHDFs (**Fig. 7C**).

Furthermore, *B. longum* RAPO CS significantly inhibited hTGF- β 1-induced α -SMA protein expression in both normal-LF (LL24) and IPF-LF (LL29) cell lines (**Fig. 7D**). In normal-LFs, *B. longum* RAPO CS partially downregulated the expression of hTGF- β 1-induced *CTGF* and *IL6*. Notably, in IPF-LFs, the CS exhibited a pronounced ability to suppress the expression of hTGF- β 1-induced pro-inflammatory genes (*IL6*, *IL1B*, and *TNFA*) rather than profibrotic genes (**Fig. 7E**). Targeted metabolomic analysis of SCFAs revealed a predominant increase in acetate levels in *B. longum* RAPO CS compared to that in control media (**Supplementary Fig. 7C**), suggesting the involvement of *B. longum* RAPO-derived acetate and its downstream metabolite, butyrate, in regulating the activation of macrophages and fibroblasts *in vivo*. Additionally, co-culture experiments demonstrated reduced α -SMA protein expression in NHDFs co-cultured with *B. longum* RAPO-treated THP-1 macrophages compared to NHDFs co-cultured with untreated THP-1 macrophages (**Supplementary Fig. 8**). Overall, these findings suggest that *B. longum* RAPO may suppress fibrosis development by directly or indirectly modulating macrophages and fibroblasts through either its intrinsic properties or secreted molecules.

DISCUSSION

This study unveiled significant alterations in antimicrobial Abs in patients with SSc, identified by changes in serum IgM Abs targeting gut microbial species. Particularly striking was the marked depletion of Abs against *B. longum* in patients with SSc. Moreover, the oral administration of *B. longum* strain RAPO effectively attenuated skin and lung fibrosis in SSc mice. These therapeutic effects were linked to the enhanced growth of SCFA-producing gut bacteria, increased fecal butyrate production, *Gpr41* activation in MLN cells, and reduced infiltration of inflammatory macrophages/monocytes, along with *Ccl2* downregulation in the fibrotic tissues and spleen. These findings provide initial evidence supporting the potential of *B. longum* RAPO as a promising probiotic for protecting against tissue fibrosis associated with SSc.

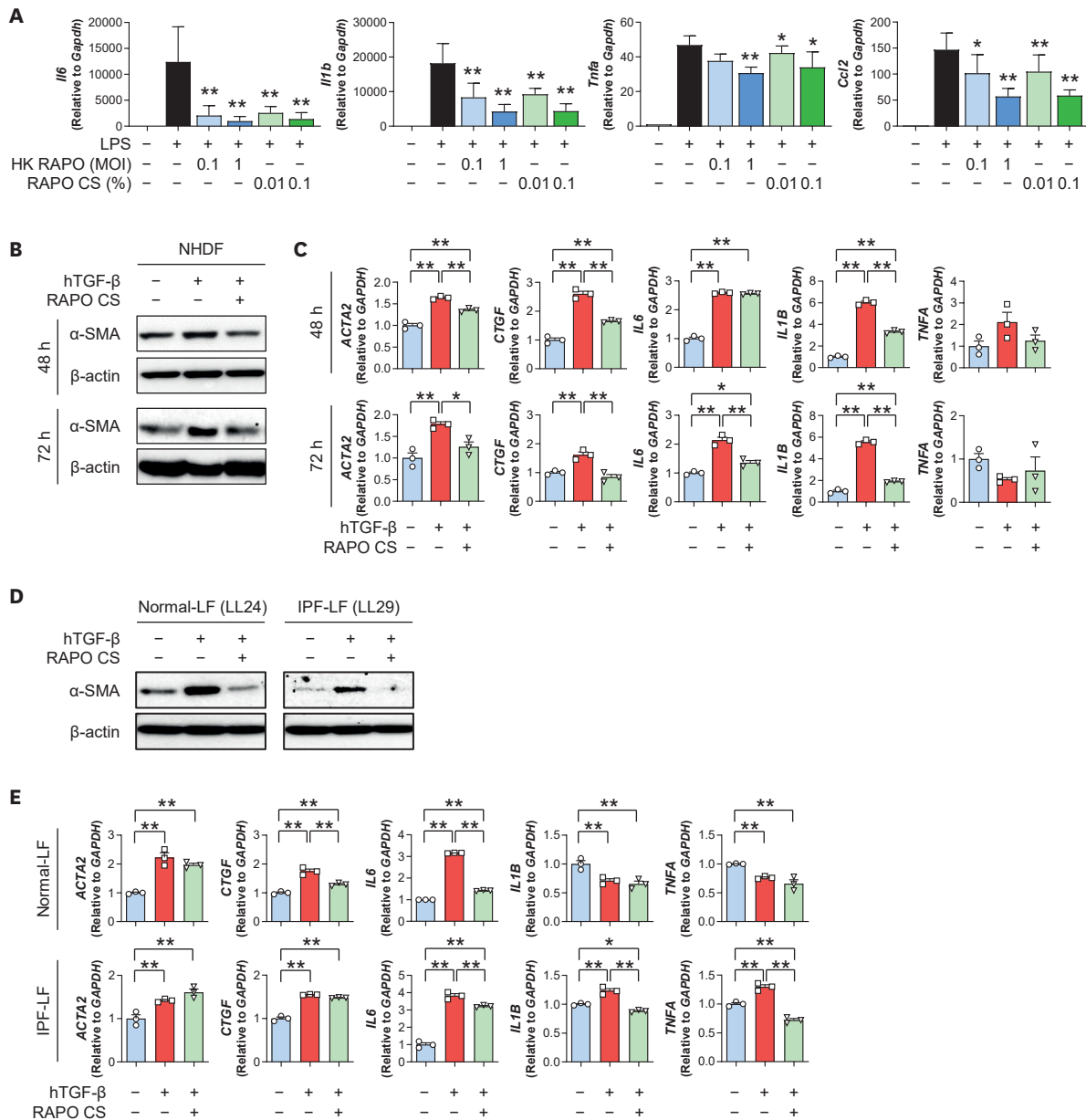


Figure 7. Modulating ability of *B. longum* RAPO and its derived components on macrophages and fibroblasts activation *in vitro*. (A) Pro-inflammatory gene expression of RAW 264.7 macrophage cells stimulated with LPS in the absence or presence of HK-*B. longum* RAPO or its CS (n=3-4/group). (B, C) α-SMA protein expression (B) and profibrotic and pro-inflammatory gene expression (C) of primary NHDFs stimulated with hTGF-β1 in the absence or presence of *B. longum* RAPO CS. (D, E) α-SMA protein expression (D) and profibrotic and pro-inflammatory gene expression (E) of normal-LFs (LL24) and IPF-LFs (LL29) stimulated with hTGF-β1 in the absence or presence of *B. longum* RAPO CS (n=3/group). Mean ± SEM, *p<0.05, **p<0.01.

Genomic methodologies are indispensable for assessing microbiome diversity; however, accurately identifying microbial species and comprehending host-microbiota interactions are still challenging, necessitating innovative strategies (25). Here, we introduced a microarray to scrutinize distinct microbial species and therapeutic targets in SSc by analyzing IgM reactions against a specifically designed gut microbiota panel in human serum samples. Systemic reactivity to microbial components reflects impaired mucosal immunity, with clinical implications (26). Elevated serum microbial Abs further emphasize the gut microbiota's role in disease pathogenesis (27). Circulating Abs against microbial peptides have been

implicated in conditions such as inflammatory bowel disease, where they are thought to arise from immune responses to luminal microbiota. Notably, these Abs correlated with more severe disease phenotypes, with a higher prevalence observed in patients with more severe Crohn's disease compared to milder forms (28). Moreover, translocated microbial ligands can activate both immune and nonimmune cells, including fibroblasts, via toll-like receptors, thereby driving fibrosis in multiple organs (27). Collectively, these findings suggest that immune responses to microbial antigens contribute to the development of fibrosis and the production of antimicrobial Abs.

Although serum Ab disturbances to gut microbiota have been documented in various diseases (29,30), specific Ab reactions against microbial antigens in SSc remain unexplored. However, fecal microbiota transplantation in SSc patients has been shown to modify IgA and IgM coating patterns and extent (31), suggesting the potential existence of gut microbiota-specific Ab responses or repertoire in the disease. While the current study could not establish a definitive relationship among antimicrobial Abs, microbial abundance, and disease severity, our findings indicate that altered Ab profiles may reflect immune responses to microbial changes and offer clues on the associations between specific microbial species and clinical symptoms.

Previous studies have highlighted gut microbial disturbances in SSc, primarily concerning gastrointestinal symptoms. Patients with mild symptoms exhibited increased levels of *Clostridium*, *Blautia*, and *Bacteroides fragilis*, while those with severe symptoms had higher *Fusobacterium* levels (6,32). Microbial profiles also varied by constipation severity, with *Lactobacillus* elevated in mild cases, *Parabacteroides* in severe cases (6). *Akkermansia muciniphila* was associated with severe diarrhea and malnutrition (33). Beyond the gut, skin microbiome alterations included elevated *Rhodotorula glutinis* in early dcSSc, decreased *Propionibacterium* and *Malassezia*, and increased gram-negative bacteria like *Burkholderia*, *Citrobacter*, and *Vibrio* in lcSSc or dcSSc patients (34,35). Furthermore, decreased microbial diversity correlated with reduced lung function and higher mortality (36). These findings underscore the value of a serum-based approach for characterizing microbiome alterations across organ systems in SSc, a disease with heterogeneous phenotypes. Robust antigen-specific Abs responsive to microbiota may provide unique insights into exploring specific microbiota members associated with SSc clinical phenotypes and their role in pathophysiology.

While IgA is the dominant Ab at mucosal sites (37), IgM also holds significance in maintaining local tolerance and influencing microbiota composition in mucosal surfaces (38). IgM can swiftly respond to external triggers as the primary humoral Ab, closely mirroring disease-relevant processes or pathogen-specific responses (39). The pentameric structure of IgM enables efficient recognition of microbial antigens through multivalent binding (40), effectively pinpointing bacteria-specific reactions at early and current disease stages. However, considering the overlaps and distinctions in the reactivities of Ab isotypes against microbiota members (41), further investigation of microbiota-specific IgA and IgG along with IgM may offer comprehensive insights into microbial alterations associated with disease progression.

In this study, we selected *B. longum* as an initial candidate for SSc treatment due to its SCFA production, which is implicated in SSc therapy (7,9), and its highest-ranked probiotic species in our bacterial microarray analysis. Recent studies have highlighted *B. longum*'s therapeutic potential in improving skin health (42) and reducing lung inflammation (43). Among 2 *B. longum* strains tested in an SSc mouse model only *B. longum* RAPO significantly

mitigated both dermal and lung fibrosis. To determine whether these effects were due to general bifidobacterial mechanisms or strain-specific properties, we compared the 2 *B. longum* strains with another probiotic *Bifidobacterium* species, *B. bifidum* BGN4, which exhibits distinct prevalence and metabolic profiles. *B. bifidum* is less abundant in adults, whereas *B. longum* is one of the most prevalent species in healthy adults, potentially reflecting differences in metabolic activity and cell adhesion properties (44,45). Notably, our findings indicated that *B. bifidum* BGN4 lacked therapeutic efficacy in SSc mice. Although the current study did not elucidate the mechanistic differences underlying the differential effects of these strains in the SSc model, our findings underscore that therapeutic attributes vary significantly among probiotic strains, necessitating careful selection. Future research is required to investigate strain-specific metabolic activities, immunomodulatory capabilities, and host-microbiome interactions to better understand the therapeutic potential of *B. longum* and other *Bifidobacterium* strains in SSc.

The anti-inflammatory effects of *B. longum* RAPO appear to depend on both species- and strain-specific properties. Among the 32 species within the *Bifidobacterium* genus, *B. longum* has demonstrated superior anti-inflammatory efficacy (46). Strain-specific comparisons, including *B. longum*, *B. adolescentis*, and *B. bifidum*, revealed that *B. longum* RAPO most effectively suppressed proinflammatory cytokines (47), highlighting the importance of strain-specific differences in reducing dermal and lung fibrosis in SSc mice. Additionally, subcellular components of bifidobacteria, such as cytoplasmic extracts, surface proteins, and supernatants, are known to elicit strain-dependent immune responses (48). For instance, *B. longum* strains exhibit varying capacities to induce IL-10 and regulate TNF- α and INF- γ , while certain *B. bifidum* strains are linked to CD8⁺ T cell activation and Th17 polarization. The lack of efficacy observed with *B. bifidum* BGN4 in this study likely reflects these differences in immune modulation.

Based on the known predominant infiltration of inflammatory monocytes/macrophages across multiple organs in humans and mice with SSc (9,49,50), we explored the potential of *B. longum* RAPO treatment to ameliorate skin and lung fibrosis in SSc mice by targeting these cells. Our findings revealed that *B. longum* RAPO administration reduced the recruitment/accumulation of inflammatory monocytes/macrophages at affected sites in SSc mice. Since monocytes/macrophages are known to drive inflammatory and fibrotic processes in SSc (51), the observed inhibition of their infiltration by *B. longum* RAPO suggests a potential mechanism for alleviating disease progression in SSc. Moreover, CCL2 likely plays a pivotal role in recruiting inflammatory monocytes/macrophages to damaged lesions in SSc. Elevated CCL2 expression has been observed in the affected skin of patients with SSc (52), with serum levels correlating with disease activity and poor survival (53). The expression of CCR2 by inflammatory monocytes/macrophages further implicates their involvement in SSc pathogenesis (24). This CCL2-CCR2 axis strongly indicates the attraction of these cells to the fibrotic niche in SSc (51), where they differentiate into effector cells and activate T cells and fibroblasts (54). Our study demonstrates that *B. longum* RAPO effectively inhibited *Ccl2* expression in fibrotic tissues and secondary lymphoid organs of SSc mice, thereby mitigating tissue fibrosis by impeding the recruitment of monocytes/macrophages to affected lesions. Furthermore, our *in vitro* experiments revealed that *B. longum* RAPO can dampen macrophage activation under inflammatory conditions by downregulating the expressions of LPS-induced *Ccl2* and pro-inflammatory cytokine genes. These findings support the notion that *B. longum* RAPO may influence disease suppression by modulating the CCL2-CCR2 loop in affected organs, involving monocytes/macrophages.

The therapeutic effects of *B. longum* RAPO in SSc may be closely linked to its acetate production, a primary end-product of *Bifidobacterium* metabolism. Acetate serves as substrate for butyrate-producing bacteria, facilitating butyrate-mediated anti-inflammatory and immunoregulatory effects in immune cells, such as macrophages (55). Our findings revealed an increased abundance of butyrate-producing genera, including *E. ruminantium*, *Ruminococcaceae*, *Allobaculum*, and *Prevotellaceae*, as well as elevated butyrate levels in the feces of *B. longum* RAPO-treated SSc mice. These observations suggest that butyrate-mediated anti-inflammatory mechanisms play a critical role in the therapeutic effects of *B. longum* RAPO.

SCFAs modulate immunity through histone deacetylases inhibition or GPCR activation (56,57). While acetylated histone H3, linked to butyrate's anti-fibrotic effects (9), was not detected in this study, we observed upregulated *Gpr41* expression in MLN cells of SSc mice treated *B. longum* RAPO. GPR41, which preferentially binds propionate and butyrate (58), has shown anti-inflammatory effects via butyrate-mediated activation in obesity treated with *B. longum subsp. infantis* (59), supporting its potential therapeutic role in the butyrate-GPR41 axis. However, in this study, *Gpr41* activation was confined to MLN, with no significant changes in GPCR gene expression in fibrotic skin and lung tissues. This suggests that *B. longum* RAPO may indirectly modulate systemic fibrotic process through immune regulation in gut-associated lymphoid tissues. Although the precise role of GPR41 in fibrosis remains unclear (60), this study highlights the enrichment of butyrate-producing gut bacteria and increased fecal butyrate production following *B. longum* RAPO treatment. These changes, coupled with *Gpr41* activation in MLN cells, suggest a mechanism by which *B. longum* RAPO influences extra-intestinal organs in SSc.

Despite the known therapeutic potential of probiotics, their mechanisms of action on extra-intestinal organs are still unclear. Our previous study in SSc mice suggested microbial metabolites influencing distant organs (9). Our current *in vitro* findings showed that *B. longum* RAPO CS suppressed pro-inflammatory gene expression in macrophages and inhibited myofibroblast transition in fibroblast cell lines, suggesting potential disease prevention in distant organs by mediating components or metabolites secreted by *B. longum* RAPO. This is consistent with prior research demonstrating the immune-modulatory effects of CS from probiotic strains (61,62). Although the precise components derived from *B. longum* RAPO and their *in vivo* kinetics were not investigated in the present study, we propose its potential to inhibit SSc development through interactions with various cell types in circulation.

This study has several limitations. First, the serum microbial array may not directly reflect the gut microbiota abundance or activity due to potential antigen cross-reactivity, requiring further validation using fecal samples in the same individuals. Second, the small sample size within each SSc clinical category limited robust correlations between clinical features and microbial species. Third, we were unable to investigate the distinct responses of *B. longum* RAPO compared to other *Bifidobacterium* species or *B. longum* strains. Reliable techniques need to be developed to assess strain-specific differences in metabolic and immunological activities *in vitro*. Fourth, while a dose of 2×10^9 CFU *B. longum* RAPO was identified as optimal for mitigating both skin and lung fibrosis in SSc mice, clear dose-dependent effects were not observed in treating these fibrotic conditions. Further studies are necessary to refine dosing strategies to better understand the mechanisms underlying tissue-specific responses and the non-linear effects of *B. longum* RAPO. Lastly, although this study proposed butyrate-mediated *Gpr41* activation as a potential mechanism underlying the therapeutic effects of *B. longum* RAPO administration, the precise role of *Gpr41* was not fully investigated. Future research is

needed to identify the specific cell types expressing *Gpr41* and clarify its functional roles in mediating the therapeutic benefits in this disease model.

In conclusion, our study has identified *B. longum* RAPO as a novel probiotic with protective effects against BLM-induced dermal and lung fibrosis. These effects are attributed to the modulation of inflammatory monocytes/macrophages and the augmentation of SCFA-producing gut bacteria. Moreover, our findings elucidate potential mechanisms underlying the efficacy of *B. longum* RAPO against SSc, suggesting its influence on extra-intestinal tissues. We propose *B. longum* RAPO as a promising probiotic candidate for SSc treatment and present a valuable strategy for targeting microbiota using a serum-based microbial microarray.

ACKNOWLEDGEMENTS

This work was supported by the National Research Foundation of Korea (NRF) grants (NRF-2020R111A3071922, NRF-2022R1F1A1071114) funded by the Korea government (<http://www.nrf.re.kr/index>).

SUPPLEMENTARY MATERIALS

Supplementary Data 1

Methods

Supplementary Table 1

Primer and probe sequences for digital PCR

Supplementary Table 2

Cell staining Abs for flow cytometry analysis

Supplementary Table 3

TaqMan assays and SBYR primer sequences for quantitative real-time PCR

Supplementary Table 4

Clinical characteristics of healthy individuals and patients with SSc

Supplementary Table 5

Pearson correlation coefficients between Ab levels against bacterial species and clinical parameters in patients with SSc

Supplementary Figure 1

LefSe analysis of serum anti-microbial Ab profile comparing patients with SSc (n=76) to HC (n=50). The histogram illustrates LDA scores of species enriched in HC and SSc in green and red, respectively ($p < 0.01$, LDA score > 2.0).

Supplementary Figure 2

Effects of *Bifidobacterium* strains on dermal fibrosis in BLM-induced SSc mice. Mice received subcutaneous injections of BLM to the dorsal skin, administered 5 times a week for 2 wk. Various doses of *B. longum* BORI and *B. bifidum* BGN4 were orally administered 2 wk before

BLM injection and subsequently continued for 4 wk. Dermal thickness was evaluated using Masson's trichrome staining of skin tissues obtained from mice in each experimental group: normal mice (n=6), non-treated SSc mice (n=13), SSc mice treated with *B. longum* BORI or *B. bifidum* BGN4 at doses of 1, 2, or 5×10^9 CFUs (n=4–7/each treated). Median \pm min to max.

Supplementary Figure 3

Flow cytometric gating strategy for macrophage (MP) subsets in bronchoalveolar lavage (BAL) cells. CD45⁺CD64⁺ MPs were subdivided into alveolar macrophages (AM, CD11c⁺CD11b⁻) and exudate macrophages (exMac, CD11c⁺CD11b⁺).

Supplementary Figure 4

Expression levels of genes associated with T cell cytokines in skin, lung, MLN, and spleen cells collected from normal (n=5), BLM-treated (n=5), and BLM/RAPO-treated (n=6) mice.

Supplementary Figure 5

Analysis of fecal samples collected from normal (n=5), BLM-induced SSc (n=5), and BLM/RAPO-treated (n=6) mice using 16S rRNA gene sequencing. The relative abundance of gut microbiota was compared between groups at the genus level and significantly different genera were visualized.

Supplementary Figure 6

Expression levels of GPCR genes in skin and lung tissues from normal (n=5), BLM-treated (n=5), and BLM/RAPO-treated (n=6) mice.

Supplementary Figure 7

(A, B) Cytotoxicity evaluation of *B. longum* RAPO or its CS on RAW 264.7 macrophages (A) and NHDFs (B) using the MTT assay. n=4–8/group for RAW cells. n=2–4/group for NHDFs. Median and interquartile range (1st–3rd quartile). #p<0.05 vs. group not exposed to LPS, HK RAPO, and its CS, *p<0.05. (C) Quantification of SCFAs in *B. longum* RAPO CS.

Supplementary Figure 8

Modulation of fibroblast activation by *B. longum* RAPO through macrophage interactions *in vitro*. THP-1 cells were differentiated into macrophages using phorbol 12-myristate 13-acetate treatment and then treated with or without HK-*B. longum* RAPO (HK RAPO). The macrophages were subsequently co-cultured with NHDFs under LPS stimulation. Alpha-SMA protein expression was analyzed in the NHDFs.

REFERENCES

1. Jeong JE, Kim SH. Clinical characteristics of juvenile systemic sclerosis in Korea: 31-year single-center study. *J Rheum Dis* 2024;31:25-32. [PUBMED](#) | [CROSSREF](#)
2. Tsou PS, Varga J, O'Reilly S. Advances in epigenetics in systemic sclerosis: molecular mechanisms and therapeutic potential. *Nat Rev Rheumatol* 2021;17:596-607. [PUBMED](#) | [CROSSREF](#)
3. Bukiri H, Volkman ER. Current advances in the treatment of systemic sclerosis. *Curr Opin Pharmacol* 2022;64:102211. [PUBMED](#) | [CROSSREF](#)
4. Lee SG, Moon KW. Epidemiology and treatment of systemic sclerosis in Korea. *J Rheum Dis* 2022;29:200-214. [PUBMED](#) | [CROSSREF](#)
5. Volkman ER. Is there a role for the microbiome in systemic sclerosis? *Expert Rev Clin Immunol* 2023;19:237-240. [PUBMED](#) | [CROSSREF](#)

6. Volkmann ER, Chang YL, Barroso N, Furst DE, Clements PJ, Gorn AH, Roth BE, Conklin JL, Getzug T, Borneman J, et al. Association of systemic sclerosis with a unique colonic microbial consortium. *Arthritis Rheumatol* 2016;68:1483-1492. [PUBMED](#) | [CROSSREF](#)
7. Plichta DR, Somani J, Pichaud M, Wallace ZS, Fernandes AD, Perugino CA, Lähdesmäki H, Stone JH, Vlamakis H, Chung DC, et al. Congruent microbiome signatures in fibrosis-prone autoimmune diseases: IgG4-related disease and systemic sclerosis. *Genome Med* 2021;13:35. [PUBMED](#) | [CROSSREF](#)
8. Mehta H, Goulet PO, Mashiko S, Desjardins J, Pérez G, Koenig M, Senécal JL, Constante M, Santos MM, Sarfati M. Early-life antibiotic exposure causes intestinal dysbiosis and exacerbates skin and lung pathology in experimental systemic sclerosis. *J Invest Dermatol* 2017;137:2316-2325. [PUBMED](#) | [CROSSREF](#)
9. Park HJ, Jeong OY, Chun SH, Cheon YH, Kim M, Kim S, Lee SI. Butyrate improves skin/lung fibrosis and intestinal dysbiosis in bleomycin-induced mouse models. *Int J Mol Sci* 2021;22:2765. [PUBMED](#) | [CROSSREF](#)
10. Strahm N, Didriksen H, Fretheim H, Molberg Ø, Midtvedt Ø, Farstad IN, Midtvedt T, Lundin KEA, Aabakken L, Blyszczuk P, et al. Effects of faecal microbiota transplantation on the small intestinal mucosa in systemic sclerosis. *Rheumatology (Oxford)* 2023;62:2918-2929. [PUBMED](#) | [CROSSREF](#)
11. Marighela TF, Arismendi MI, Marville V, Brunialti MKC, Salomão R, Kayser C. Effect of probiotics on gastrointestinal symptoms and immune parameters in systemic sclerosis: a randomized placebo-controlled trial. *Rheumatology (Oxford)* 2019;58:1985-1990. [PUBMED](#) | [CROSSREF](#)
12. Hoffmann-Vold AM, Fretheim HH, Sarna VK, Barua I, Carstens MN, Distler O, Khanna D, Volkmann ER, Midtvedt Ø, Didriksen H, et al. Safety and efficacy of faecal microbiota transplantation by Anaerobic Cultivated Human Intestinal Microbiome (ACHIM) in patients with systemic sclerosis: study protocol for the randomised controlled phase II ReSScue trial. *BMJ Open* 2021;11:e048541. [PUBMED](#) | [CROSSREF](#)
13. Balakrishnan B, Luckey D, Bodhke R, Chen J, Marietta E, Jeraldo P, Murray J, Taneja V. *Prevotella histicola* protects from arthritis by expansion of *Allobaculum* and augmenting butyrate production in humanized mice. *Front Immunol* 2021;12:609644. [PUBMED](#) | [CROSSREF](#)
14. Scher JU, Sczesnak A, Longman RS, Segata N, Ubeda C, Bielski C, Rostron T, Cerundolo V, Pamer EG, Abramson SB, et al. Expansion of intestinal *Prevotella copri* correlates with enhanced susceptibility to arthritis. *Elife* 2013;2:e01202. [PUBMED](#) | [CROSSREF](#)
15. Wensel CR, Pluznick JL, Salzberg SL, Sears CL. Next-generation sequencing: insights to advance clinical investigations of the microbiome. *J Clin Invest* 2022;132:e154944. [PUBMED](#) | [CROSSREF](#)
16. Li J, Zhai X, Ding C, Liu Y, Dong Q, Xu D, Wang X, Qiu J, Zhang Q, Pan J, et al. Development of a bacterial macroarray for the rapid screening of targeted antibody-secreted hybridomas. *SLAS Discov* 2019;24:190-198. [PUBMED](#) | [CROSSREF](#)
17. Campanero-Rhodes MA, Lacombe A, Prat C, García E, Solís D. Development and evaluation of a microarray platform for detection of serum antibodies against *Streptococcus pneumoniae* capsular polysaccharides. *Anal Chem* 2020;92:7437-7443. [PUBMED](#) | [CROSSREF](#)
18. Lee SH, Turpin W, Espin-García O, Raygoza Garay JA, Smith MI, Leibovitz H, Goethel A, Turner D, Mack D, Deslandres C, et al. Anti-microbial antibody response is associated with future onset of Crohn's disease independent of biomarkers of altered gut barrier function, subclinical inflammation, and genetic risk. *Gastroenterology* 2021;161:1540-1551. [PUBMED](#) | [CROSSREF](#)
19. Thirumalapura NR, Ramachandran A, Morton RJ, Malayer JR. Bacterial cell microarrays for the detection and characterization of antibodies against surface antigens. *J Immunol Methods* 2006;309:48-54. [PUBMED](#) | [CROSSREF](#)
20. Campanero-Rhodes MA, Palma AS, Menéndez M, Solís D. Microarray strategies for exploring bacterial surface glycans and their interactions with glycan-binding proteins. *Front Microbiol* 2020;10:2909. [PUBMED](#) | [CROSSREF](#)
21. Kim S, Chun SH, Cheon YH, Kim M, Kim HO, Lee H, Hong ST, Park SJ, Park MS, Suh YS, et al. *Peptoniphilus gorbachii* alleviates collagen-induced arthritis in mice by improving intestinal homeostasis and immune regulation. *Front Immunol* 2024;14:1286387. [PUBMED](#) | [CROSSREF](#)
22. Hübner RH, Gitter W, El Mokhtari NE, Mathiak M, Both M, Bolte H, Freitag-Wolf S, Bewig B. Standardized quantification of pulmonary fibrosis in histological samples. *Biotechniques* 2008;44:507-517. [PUBMED](#) | [CROSSREF](#)
23. Rivière A, Selak M, Lantin D, Leroy F, De Vuyst L. Bifidobacteria and butyrate-producing colon bacteria: importance and strategies for their stimulation in the human gut. *Front Microbiol* 2016;7:979. [PUBMED](#) | [CROSSREF](#)
24. Mysore V, Tahir S, Furuhashi K, Arora J, Rosetti F, Cullere X, Yazbeck P, Sekulic M, Lemieux ME, Raychaudhuri S, et al. Monocytes transition to macrophages within the inflamed vasculature via monocyte CCR2 and endothelial TNFR2. *J Exp Med* 2022;219:e20210562. [PUBMED](#) | [CROSSREF](#)

25. Vujkovic-Cvijin I, Welles HC, Ha CWY, Huq L, Mistry S, Brenchley JM, Trinchieri G, Devkota S, Belkaid Y. The systemic anti-microbiota IgG repertoire can identify gut bacteria that translocate across gut barrier surfaces. *Sci Transl Med* 2022;14:eabl3927. [PUBMED](#) | [CROSSREF](#)
26. Papp M, Norman GL, Vitalis Z, Tornai I, Altorjay I, Foldi I, Udvardy M, Shums Z, Dinya T, Orosz P, et al. Presence of anti-microbial antibodies in liver cirrhosis--a tell-tale sign of compromised immunity? *PLoS One* 2010;5:e12957. [PUBMED](#) | [CROSSREF](#)
27. Watanabe D, Kamada N. Contribution of the gut microbiota to intestinal fibrosis in Crohn's disease. *Front Med (Lausanne)* 2022;9:826240. [PUBMED](#) | [CROSSREF](#)
28. Rieder F. The gut microbiome in intestinal fibrosis: environmental protector or provocateur? *Sci Transl Med* 2013;5:190ps10. [PUBMED](#) | [CROSSREF](#)
29. Christmann BS, Abrahamsson TR, Bernstein CN, Duck LW, Mannon PJ, Berg G, Björkstén B, Jenmalm MC, Elson CO. Human seroreactivity to gut microbiota antigens. *J Allergy Clin Immunol* 2015;136:1378-1386.e1-5. [PUBMED](#) | [CROSSREF](#)
30. Zeng MY, Cisalpino D, Varadarajan S, Hellman J, Warren HS, Cascalho M, Inohara N, Núñez G. Gut microbiota-induced immunoglobulin G controls systemic infection by symbiotic bacteria and pathogens. *Immunity* 2016;44:647-658. [PUBMED](#) | [CROSSREF](#)
31. Fretheim H, Chung BK, Didriksen H, Bækkevold ES, Midtvedt Ø, Brunborg C, Holm K, Valeur J, Tennøe AH, Garen T, et al. Fecal microbiota transplantation in systemic sclerosis: a double-blind, placebo-controlled randomized pilot trial. *PLoS One* 2020;15:e0232739. [PUBMED](#) | [CROSSREF](#)
32. Volkmann ER, Hoffmann-Vold AM, Chang YL, Jacobs JP, Tillisch K, Mayer EA, Clements PJ, Hov JR, Kummén M, Midtvedt Ø, et al. Systemic sclerosis is associated with specific alterations in gastrointestinal microbiota in two independent cohorts. *BMJ Open Gastroenterol* 2017;4:e000134. [PUBMED](#) | [CROSSREF](#)
33. Natalello G, Bosello SL, Paroni Sterbini F, Posteraro B, De Lorenzis E, Canestrari GB, Gigante L, Verardi L, Ferraccioli G, Sanguinetti M, et al. Gut microbiota analysis in systemic sclerosis according to disease characteristics and nutritional status. *Clin Exp Rheumatol* 2020;38 Suppl 125:73-84. [PUBMED](#)
34. Arron ST, Dimon MT, Li Z, Johnson ME, Wood TA, Feeney L, Angeles JG, Lafyatis R, Whitfield ML. High *Rhodotorula* sequences in skin transcriptome of patients with diffuse systemic sclerosis. *J Invest Dermatol* 2014;134:2138-2145. [PUBMED](#) | [CROSSREF](#)
35. Johnson ME, Franks JM, Cai G, Mehta BK, Wood TA, Archambault K, Pioli PA, Simms RW, Orzechowski N, Arron S, et al. Microbiome dysbiosis is associated with disease duration and increased inflammatory gene expression in systemic sclerosis skin. *Arthritis Res Ther* 2019;21:49. [PUBMED](#) | [CROSSREF](#)
36. Takahashi Y, Saito A, Chiba H, Kuronuma K, Ikeda K, Kobayashi T, Ariki S, Takahashi M, Sasaki Y, Takahashi H. Impaired diversity of the lung microbiome predicts progression of idiopathic pulmonary fibrosis. *Respir Res* 2018;19:34. [PUBMED](#) | [CROSSREF](#)
37. Nakajima A, Vogelzang A, Maruya M, Miyajima M, Murata M, Son A, Kuwahara T, Tsuruyama T, Yamada S, Matsuura M, et al. IgA regulates the composition and metabolic function of gut microbiota by promoting symbiosis between bacteria. *J Exp Med* 2018;215:2019-2034. [PUBMED](#) | [CROSSREF](#)
38. Magri G, Comerma L, Pybus M, Sintés J, Lligé D, Segura-Garzón D, Bascones S, Yeste A, Grasset EK, Gutzeit C, et al. Human secretory IgM emerges from plasma cells clonally related to gut memory B cells and targets highly diverse commensals. *Immunity* 2017;47:118-134.e8. [PUBMED](#) | [CROSSREF](#)
39. Boonstra M, Bakker JA, Grummels A, Ninaber MK, Ajmone Marsan N, Wortel CM, Huizinga TWJ, Jordan S, Hoffman-Vold AM, Distler O, et al. Association of anti-topoisomerase I antibodies of the IgM isotype with disease progression in anti-topoisomerase I-positive systemic sclerosis. *Arthritis Rheumatol* 2020;72:1897-1904. [PUBMED](#) | [CROSSREF](#)
40. Jones K, Savulescu AF, Brombacher F, Hadebe S. Immunoglobulin M in health and diseases: how far have we come and what next? *Front Immunol* 2020;11:595535. [PUBMED](#) | [CROSSREF](#)
41. Sterlin D, Fadlallah J, Slack E, Gorochoy G. The antibody/microbiota interface in health and disease. *Mucosal Immunol* 2020;13:3-11. [PUBMED](#) | [CROSSREF](#)
42. Fang Z, Pan T, Li L, Wang H, Zhu J, Zhang H, Zhao J, Chen W, Lu W. *Bifidobacterium longum* mediated tryptophan metabolism to improve atopic dermatitis via the gut-skin axis. *Gut Microbes* 2022;14:2044723. [PUBMED](#) | [CROSSREF](#)
43. MacSharry J, O'Mahony C, Shalaby KH, Sheil B, Karmouty-Quintana H, Shanahan F, Martin JG. Immunomodulatory effects of feeding with *Bifidobacterium longum* on allergen-induced lung inflammation in the mouse. *Pulm Pharmacol Ther* 2012;25:325-334. [PUBMED](#) | [CROSSREF](#)
44. Derrien M, Turroni F, Ventura M, van Sinderen D. Insights into endogenous *Bifidobacterium* species in the human gut microbiota during adulthood. *Trends Microbiol* 2022;30:940-947. [PUBMED](#) | [CROSSREF](#)
45. Devika NT, Raman K. Deciphering the metabolic capabilities of Bifidobacteria using genome-scale metabolic models. *Sci Rep* 2019;9:18222. [PUBMED](#) | [CROSSREF](#)

46. Oh DK, Na HS, Jhun JY, Lee JS, Um IG, Lee SY, Park MS, Cho ML, Park SH. *Bifidobacterium longum* BORI inhibits pain behavior and chondrocyte death, and attenuates osteoarthritis progression. *PLoS One* 2023;18:e0286456. [PUBMED](#) | [CROSSREF](#)
47. Jeong Y, Jhun J, Lee SY, Na HS, Choi J, Cho KH, Lee SY, Lee AR, Park SJ, You HJ, et al. Therapeutic potential of a novel *Bifidobacterium* identified through microbiome profiling of RA patients with different RF levels. *Front Immunol* 2021;12:736196. [PUBMED](#) | [CROSSREF](#)
48. Ruiz L, Delgado S, Ruas-Madiedo P, Sánchez B, Margolles A. Bifidobacteria and their molecular communication with the immune system. *Front Microbiol* 2017;8:2345. [PUBMED](#) | [CROSSREF](#)
49. Gong P, Ding Y, Sun R, Jiang Z, Li W, Su X, Tian R, Zhou Y, Wang T, Jiang J, et al. Mesenchymal stem cells alleviate systemic sclerosis by inhibiting the recruitment of pathogenic macrophages. *Cell Death Dis* 2022;8:466. [PUBMED](#) | [CROSSREF](#)
50. Toledo DM, Pioli PA. Macrophages in systemic sclerosis: novel insights and therapeutic implications. *Curr Rheumatol Rep* 2019;21:31. [PUBMED](#) | [CROSSREF](#)
51. Al-Adwi Y, Westra J, van Goor H, Burgess JK, Denton CP, Mulder DJ. Macrophages as determinants and regulators of fibrosis in systemic sclerosis. *Rheumatology (Oxford)* 2023;62:535-545. [PUBMED](#) | [CROSSREF](#)
52. Mathes AL, Christmann RB, Stifano G, Affandi AJ, Radstake TR, Farina GA, Padilla C, McLaughlin S, Lafyatis R. Global chemokine expression in systemic sclerosis (SSc): CCL19 expression correlates with vascular inflammation in SSc skin. *Ann Rheum Dis* 2014;73:1864-1872. [PUBMED](#) | [CROSSREF](#)
53. Wu M, Baron M, Pedroza C, Salazar GA, Ying J, Charles J, Agarwal SK, Hudson M, Pope J, Zhou X, et al. Ccl2 in the circulation predicts long-term progression of interstitial lung disease in patients with early systemic sclerosis: data from two independent cohorts. *Arthritis Rheumatol* 2017;69:1871-1878. [PUBMED](#) | [CROSSREF](#)
54. Bhandari R, Ball MS, Martyanov V, Popovich D, Schaafsma E, Han S, ElTanbouly M, Orzechowski NM, Carns M, Arroyo E, et al. Profibrotic activation of human macrophages in systemic sclerosis. *Arthritis Rheumatol* 2020;72:1160-1169. [PUBMED](#) | [CROSSREF](#)
55. Flint HJ, Duncan SH, Scott KP, Louis P. Links between diet, gut microbiota composition and gut metabolism. *Proc Nutr Soc* 2015;74:13-22. [PUBMED](#) | [CROSSREF](#)
56. Lee C, Lee H, Park JC, Im SH. Microbial components and effector molecules in T helper cell differentiation and function. *Immune Netw* 2023;23:e7. [PUBMED](#) | [CROSSREF](#)
57. Li M, van Esch BCAM, Wagenaar GTM, Garssen J, Folkerts G, Henricks PAJ. Pro- and anti-inflammatory effects of short chain fatty acids on immune and endothelial cells. *Eur J Pharmacol* 2018;831:52-59. [PUBMED](#) | [CROSSREF](#)
58. He M, Shi B. Gut microbiota as a potential target of metabolic syndrome: the role of probiotics and prebiotics. *Cell Biosci* 2017;7:54. [PUBMED](#) | [CROSSREF](#)
59. Kou R, Wang J, Li A, Wang Y, Zhang B, Liu J, Sun Y, Wang S. Ameliorating Effects of *Bifidobacterium longum* subsp. *infantis* FB3-14 against high-fat-diet-induced obesity and gut microbiota disorder. *Nutrients* 2023;15:4104. [PUBMED](#) | [CROSSREF](#)
60. Trompette A, Gollwitzer ES, Yadava K, Sichelstiel AK, Sprenger N, Ngom-Bru C, Blanchard C, Junt T, Nicod LP, Harris NL, et al. Gut microbiota metabolism of dietary fiber influences allergic airway disease and hematopoiesis. *Nat Med* 2014;20:159-166. [PUBMED](#) | [CROSSREF](#)
61. Bermudez-Brito M, Muñoz-Quezada S, Gomez-Llorente C, Matencio E, Bernal MJ, Romero F, Gil A. Cell-free culture supernatant of *Bifidobacterium breve* CNCM I-4035 decreases pro-inflammatory cytokines in human dendritic cells challenged with *Salmonella typhi* through TLR activation. *PLoS One* 2013;8:e59370. [PUBMED](#) | [CROSSREF](#)
62. Yang KM, Kim JS, Kim HS, Kim YY, Oh JK, Jung HW, Park DS, Bae KH. *Lactobacillus reuteri* AN417 cell-free culture supernatant as a novel antibacterial agent targeting oral pathogenic bacteria. *Sci Rep* 2021;11:1631. [PUBMED](#) | [CROSSREF](#)